Mie-Resonant Nanophotonics and Metasurfaces

Yuri Kivshar

Nonlinear Physics Center, Research School of Physics, Australian National University, Canberra ACT 2601, Australia

E-mail: yuri.kivshar@anu.edu.au

Recent progress is metaphotonics is driven by the physics of Mie resonances excited in high-index dielectric nanoparticles and voids created in dielectric media. This provides a novel platform for localization of light in subwavelength photonic structures and opens new horizons for metamaterial-enabled photonics, or metaphotonics. Recently emerged field of Mie-resonant metaphotonics (also called "Mie-tronics") employs resonances in high-index dielectric nanoparticles and dielectric metasurfaces and aiming for novel applications of the subwavelength optics and photonics. High-index subwavelength resonant dielectric structures emerged recently as a new platform for nanophotonics [1]. They benefit from low material losses and provide a simple way to realize magnetic response which enables efficient flat-optics devices reaching and even outperforming the capabilities of bulk components. Here we aim to review the physics of Mie resonances and photonic bound states in the continuum (BICs) and their applications in metaphotonics and metasurfaces, including enhancement of light-matter interaction for nonlinear and topological metadevices, and the development of active nanophotonic devices and nanolasers.

Figure 1 display the major physical effects associate with the multipolar Mie resonances of individual dielectric nanoparticles, and Fig. 2 shows examples of the Mie-resonant structures and some of their functionalities.

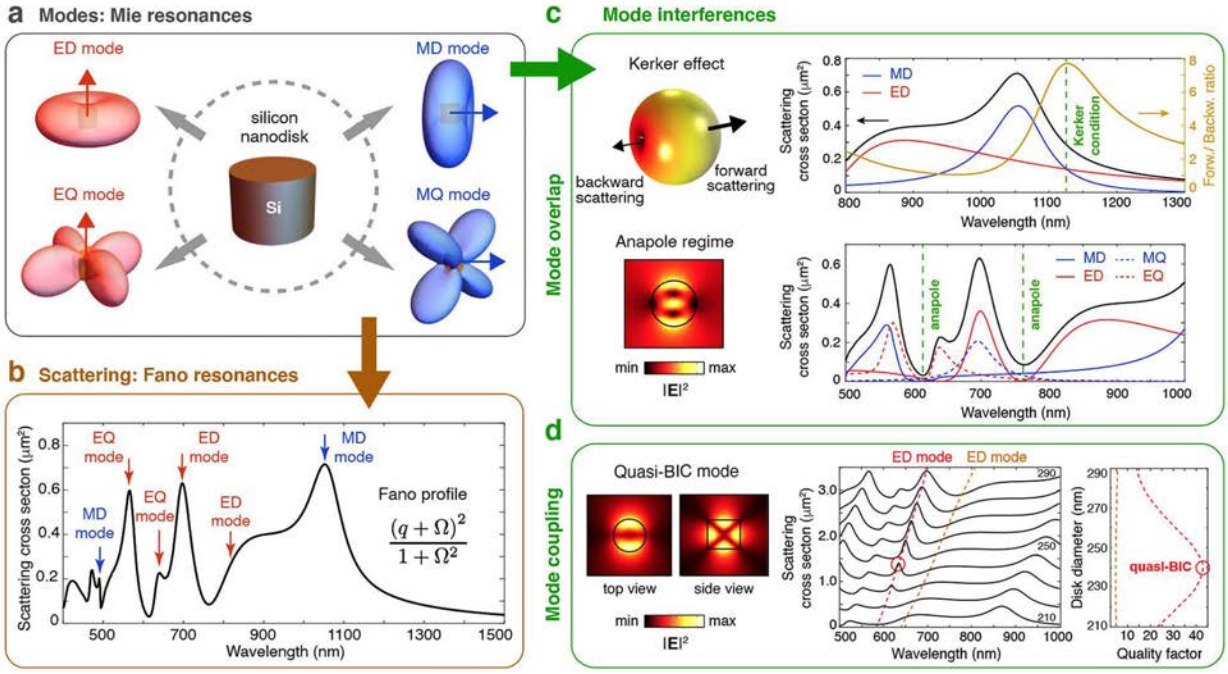

Figure 1. Mie resonances of individual dielectric nanoparticles and their interferences. (a) Schematic of a Si nanodisk and radiation patterns of its fundamental modes: electric dipole and quadrupole (ED and EQ, red), and magnetic dipole and quadrupole (MD and MQ, blue). (b) Characteristic scattering spectrum of a Si nanodisk excited by a normally incident plane wave. Each Mie mode is manifested with an asymmetric resonant peak with a Fano profile. The resonant wavelengths of electric and magnetic Mie resonances are shown with red and blue arrows, respectively. (c) Mode interferences due to nonresonant mode overlap: the Kerker effect with increased forward directionality of the scattered field and the anapole regime with the near-field enhancement and suppressed far-field scattered signal. (d) Formation of a quasi-BIC mode with increased Q factor due to a strong coupling between two ED modes. Scattering spectra for different disk diameters. The spectra are shifted relatively by 0.35 μm^2. The Q factor of neighbouring ED modes vs disk diameter.

Bound states in the continuum (BICs) are associated with the embedded eigenvalues, and they are of a considerable scientific interest because they can provide an important physical mechanism for trapping electromagnetic energy in open resonators for long time. In practice, BIC can be realized as quasi-BIC, being directly associated with the so-called supercavity mode, where both the Q factor and the resonance width become finite. BIC-inspired localization of light makes it possible to realize high-Q modes in photonic structures such as nanoantennas and metasurfaces.

The author acknowledges a support from the Australian Research Council (grants DP200101168 and DP210101292).

Reference

[1] K. Koshelev and Y. Kivshar, Dielectric resonant metaphotonics, *ACS Photonics* **8**, 102-112 (2021).

Optical and Electronic Fourier Surfaces

Nolan Lassaline[1], Raphael Brechbühler[1], Deepankur Thureja[2], Sander J. W. Vonk[1,3], Korneel Ridderbeek[1], Martin Spieser[4], Samuel Bisig[4], Boris le Feber[1], Thibault Chervy[2,5], Daniel Petter[1], Puneet A. Murthy[2], Armin W. Knoll[6], Freddy T. Rabouw[1,3], David J. Norris[1]

1. Optical Materials Engineering Laboratory, ETH Zurich, Zurich, Switzerland
2. Quantum Photonics Group, ETH Zurich, Zurich, Switzerland
3. Debye Institute for Nanomaterials Science, Utrecht University, Utrecht, The Netherlands
4. Heidelberg Instruments Nano/SwissLitho, Zurich, Switzerland
5. NTT Research, Inc., Sunnyvale, California, USA
6. IBM Research – Zurich, Rueschlikon, Switzerland

E-mail: dnorris@ethz.ch

Gratings and holograms are patterned surfaces that tailor optical signals by diffraction. Despite the long history of such structures, variants with remarkable functionalities continue to be discovered. Further advances could exploit Fourier optics, which specifies the surface pattern that generates a desired diffracted output through its Fourier transform. The required surface profile should contain a precise sum of sinusoidal waves, each with a well-defined amplitude, spatial frequency, and phase, to shape the optical wavefront. However, because fabrication techniques typically yield profiles with at most a few depth levels, complex "wavy" surfaces cannot be obtained, limiting the straightforward mathematical design and implementation of sophisticated diffractive optics. In this presentation, we will discuss a simple yet powerful approach to eliminate this design–fabrication mismatch by demonstrating optical surfaces that contain an arbitrary number of specified sinusoids [1]. Multicomponent linear gratings allow precise manipulation of the dispersion, stopbands, and coupling of electromagnetic signals. More broadly, we analytically design and accurately replicate intricate two-dimensional Moiré patterns, quasicrystals, and holograms, demonstrating a variety of previously impossible diffractive surfaces (Fig. 1a). Finally, we show that such patterns can be reduced to nanometer length scales, creating wavy Fourier surfaces for 2D electronics (Fig. 1b) [2]. Therefore, this approach provides benefit for optical devices and emerging topics in photonics and 2D optoelectronics.

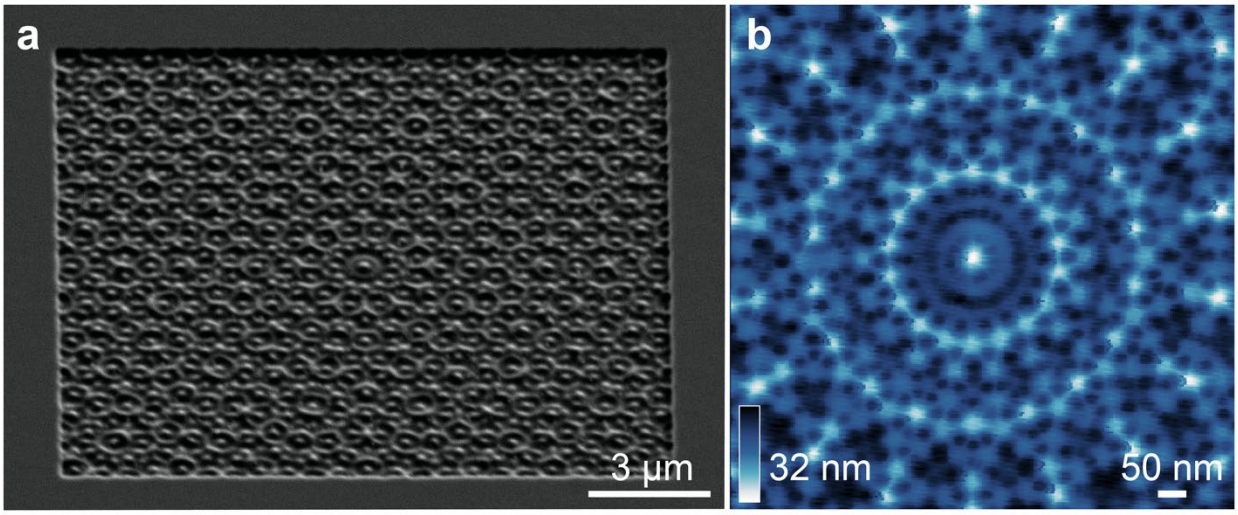

Fig. 1 Examples of optical and electronic Fourier surfaces. (a) Optical Fourier surface fabricated in silicon as a Moiré interference pattern constructed from 12 overlapping sinusoids. (b) Electronic Fourier surface fabricated in a hexagonal boron nitride (hBN) flake as a Moiré interference pattern constructed from 9 overlapping sinusoids.

References

[1] Lassaline, N., Brechbühler, R., Vonk, S. J. W., Ridderbeek, K., Spieser, M., Bisig, S., le Feber, B., Rabouw, F. T., Norris, D. J. 2020 *Nature* 582, 506–510.

[2] Lassaline, N., Thureja, D., Chervy, T., Petter, D., Murthy, P. A., Knoll, A. W., Norris, D. J. 2021 *Nano Lett.* 21, 8175–8181.

High Q-factor coupled Fabry-Perot plasmonic nanoresonator : description and applications

B. Fix[1], J. Jaeck[1],P. Bouchon[1], N. Bardou[2], B. Vest[1] and R. Haïdar[1]
[1] DOTA,ONERA,Université Paris Saclay F-91123 Palaiseau – France
[2] Center for Nanoscience and Nanotechnology (C2N)-CNRS, Université Paris-Saclay, 91128 Palaiseau, France
baptiste.fix@onera.fr

Fabry-Perot (FP) like resonances have been widely described in nanoantennas. In the case of combination of nanoantennas, it has been reported that each cavity behaves independently. Here, we evidence the interferences between two FP absorbing nanoantennas, which has a strong impact on the optical behavior. While the resonance wavelength is only slightly shifted, the level of absorption reaches nearly 100%. Moreover, the quality factor increases up to factor 7 and can be chosen by geometric design over a range from 11 to 75. We first demonstrate thanks to a simple analytical model that this coupling can be ascribed to a double FP cavity resonance, with the unique feature that each cavity is separately coupled to the outer medium. Based on this principle, we experimentally illustrate the existence of a high-Q factor resonance originating from the interference between two under-coupled ribbon-shaped nano Fabry-Perot.

The Fabry-Perot (FP) interferometer consists of two parallel highly reflecting mirrors leading dips in the reflection spectra [1]. The development of nanophotonics has given birth to FP-like nanoresonators [2]–[3], in which a guided mode in a metallic cavity has a behavior that is well described by the FP formalism. The advantages of these nanoresonators are their compactness, and the possibility to combine them, usually with negligible influences on each other [4]–[6], to design broadband or multiband resonances for applications ranging from thermal emission [7] to infrared detection[8]. Yet, they suffer from their low quality factor.

In this letter, we introduce double cavity Fabry-Perot like nanoresonators in both vertical (slit) and horizontal (ribbon) configurations. It gives birth to a spectacular effect where critical coupling, *i.e.* a zero of reflectivity, is obtained while, independently, each of the two cavities is loosely-coupled to free space. Moreover, the quality factor of the double cavity resonators is increased from 11 to 50, well beyond the limit for FP plasmonic nanoresonator [6].

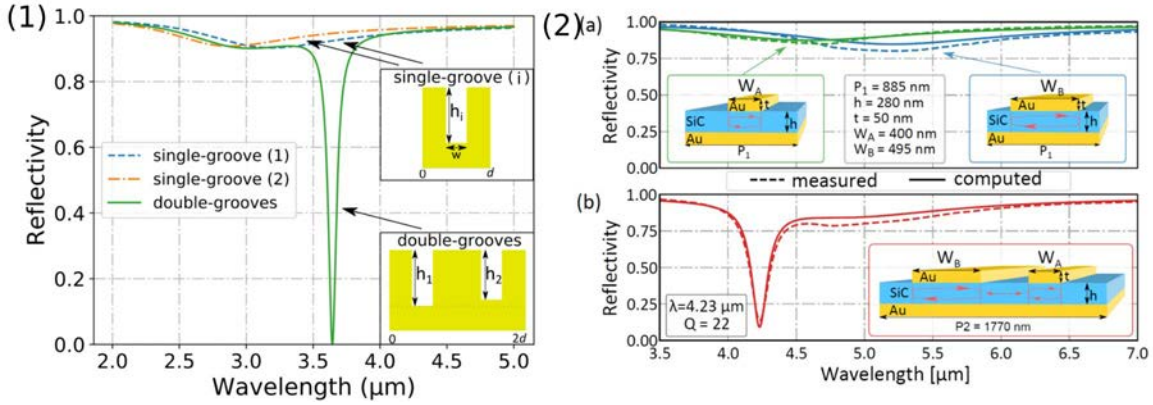

Figure 1 Comparison between the reflectivity of two loosely-coupled single-nanogroove resonators and of a critically coupled resonator composed of the two aforementioned cavities. The cavities are described in the insets (d=1µm, w=0.3µm, h1=0.62µm, h2=0.55µm). (2) Measured (dotted) and computed (plain) reflection spectra of (a) single-FP structures and (b) the coupled nano FP structure.

We developed an analytical model that confirms the multimirror FP behavior [9] and experimentally demonstrated the coupled Fabry-Perot resonance on horizontal nanoresonators [10]. We extended the description to multi coupled Fabry-Perot resonant structures with either 1D or 2D geometries and detailed some applications for non-linear emission, infrared photodetection and THz filters.

The description of the coupled nano Fabry-Perot paves the way to the manipulation and the engineering of coupling in multi-resonant nanostructures. Moreover, the resonators easily scaled geometry is also very promising for many practical applications from the near-infrared to the mm wave domain.

REFERENCES

[1] C. Fabry and A. Perot, *Ann Chim Phys*, 16,7, 1899.
[2] J. A. Porto *et al.*,*Phys. Rev. Lett.*, vol. 83, 14, 1999.
[3] E. Cubukcu *et al.*, *Appl. Phys. Lett.*, vol. 95, 20, 2009.
[4] X. Liu *et al.*, *Phys. Rev. Lett.*, vol. 104, no. 20, 2010.
[5] P. Bouchon *et al.*, *Opt. Lett.*, vol. 37, no. 6, 2012.
[6] C. Koechlin *et al.*, *Opt. Express*, vol. 21, no. 6, 2013.
[7] M. Makhsiyan *et al.*, *Appl. Phys. Lett.*, 107, 25, 2015.
[8] M. W. Knight *et al.*, *Science*, 332, 6030, May 2011.
[9] B. Fix, *et al.*," Opt. Lett. **42**, 5062-5065, 2017
[10] B. Fix, *et al.*, arXiv:2011.05242

Ultrafast infrared nano-imaging of far-from-equilibrium dynamics

Jun Nishida, Samuel C. Johnson, Peter T.S. Chang, Dylan M. Wharton, S.A. Dönges, O. Khatib, and Markus B. Raschke

Department of Physics and JILA, University of Colorado, Boulder, 2000 Colorado Ave, CO 80309, USA

E-mail: markus.raschke@colorado.edu

Quantum phase transitions, polaronic carrier transport, coherent vibrations driving singlet fission, or electronic energy transfer in light-harvesting complexes emerge from the interplay of the elementary electronic, vibrational, and phononic quantum states. By exciting one of these degrees of freedom out of equilibrium and probing their dynamic response, ultrafast spectroscopy disentangles mode-coupling and competing interactions that are otherwise convoluted in static spectroscopy. *Ultrafast infrared nano-imaging* has demonstrated access to ultrafast carrier dynamics on the nanoscale in semiconductor, correlated-electron, or polaritonic materials. However, mostly limited to strong and short-lived carrier and collective polaritonic excitations, the contrast obtained to date has remained insufficient to probe with excited state specificity the broader range of long-lived excitations, which arise from many-body interactions induced by strong perturbation among charge carriers, lattice phonons, or molecular vibrations.

Here, we demonstrate a generalizable approach to ultrafast nano-imaging based on non-degenerate *heterodyne* pump-probe infrared scattering scanning near-field optical microscopy (HPP IR *s*-SNOM) with low repetition-rate *modulated excitation*, which provides simultaneous space, time, frequency, and phase resolutions with high sensitivity (Fig. 1A) [1]. A modulated femtosecond pump pulse drives the system into an excited state, followed by infrared heterodyne probing of the transient low-energy electronic and vibrational response. The induced *third-order nano-localized polarization* is isolated by sideband lock-in detection and directly detected interferometrically in the time-domain, enabling ultrafast nano-imaging with high contrast even with low-repetition excitation. Excitation-modulated HPP IR *s*-SNOM thus provides the time-resolved analogue of ground-state nano-FTIR spectroscopy, selectively resolving the transient and nano-localized *excited-state response*.

As a representative application to quantum materials, we perform nano-imaging of the electron dynamics associated with the ultrafast photoinduced insulator-to-metal transition (IMT) in vanadium dioxide (VO_2), resolving transient domain dynamics (Fig. 1B) that is distinct from the established strain-induced heterogeneity in the thermally induced transition. In another application to molecular materials, we directly resolve heterogeneity in polaron-cation coupling that controls the photovoltaic response by probing the excited state vibrational dynamics in a triple cation perovskite (Fig. 1C-D). These examples show how heterodyne pump-probe nano-spectroscopy and -imaging with low-repetition allows for ultrafast nano-imaging of elementary processes in quantum and molecular materials in space and time.

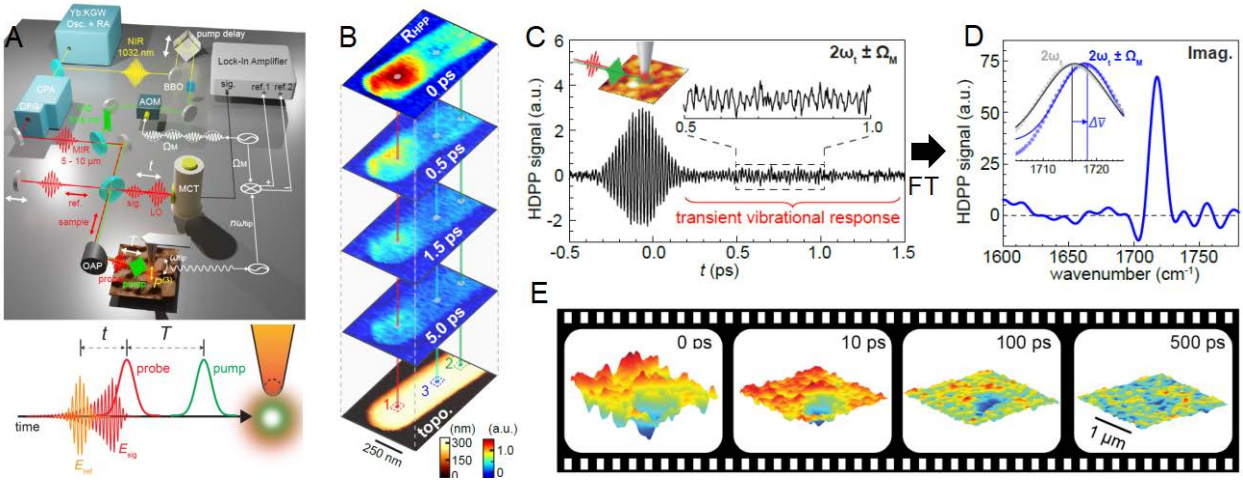

Fig. 1. (A) Ultrafast pump-probe nano-imaging with far-from equilibrium excitation and interferometric heterodyne near-field detection (HPP IR s-SNOM) for quantitative excited state contrast. (B) Example of nano-imaging the ultrafast insulator-to-metal transition in VO_2. (C,D) Ultrafast local probe nano-spectroscopy of triple-cation perovskite resolving excited state vibrational dynamics. (E) Ultrafast movie resolving associated transient heterogeneity of polaron-lattice dynamics.

References

[1] J. Nishida et al. *"Ultrafast infrared nano-imaging of far-from-equilibrium carrier and vibrational dynamics"*, Nature Commun. (in press).

Nonlinear nano-imaging of few-fs coherent dynamics in 2D graphene-semiconductor heterostructures

Wenjin Luo[1,2], Renkang Song[2], Benjamin G. Whetten[1], Xinbin Cheng[2], Alexey Belyanin[3], Tao Jiang[2,*], and Markus B. Raschke[1,*]

1. Department of Physics, and JILA, University of Colorado, Boulder, CO 80303, USA.
2. MOE Key Laboratory of Advanced Micro-Structured Materials, Shanghai Research Institute for Intelligent Autonomous Systems, and School of Physics Science and Engineering, Tongji University, Shanghai, China.
3. Department of Physics and Astronomy, Texas A&M University, College Station, TX 77843, USA.
E-mail: tjiang@tongji.edu.cn; markus.raschke@colorado.edu

Layer-stacked two-dimensional (2D) heterostructures open new avenues for the design of a wide range of novel photonic and quantum devices with properties determined by orientation-dependent interlayer coupling, band structure engineering, and sensitive external electric, magnetic, and optical control. However, the underlying mechanism of coupling, charge and energy transfer, coherent dynamics, population lifetimes, and their sensitivity with respect to spatial heterogeneities at defects, edges, and grain boundaries, are still poorly understood.

Here, we demonstrate tip-enhanced nonlinear nano-imaging with grating-coupled plasmonic nanofocusing, providing access to the desired few-nanometer spatial and few-femtosecond temporal regimes to separate competing intra- and interlayer processes, as illustrated in **Fig. 1a** [1-3]. In simultaneous nonlinear coherent broadband four-wave mixing (FWM) and incoherent 2-photon photoluminescence (2PPL) measurements, we probe graphene and WSe_2 monolayers and their heterostructures as shown in **Fig. 1b-e**. The observed nano-localized 2PPL and FWM spectra in WSe_2 and WSe_2/graphene contrast that of a pure FWM response for graphene with distinct underlying near-field-coupled enhancement and quenching of FWM and 2PPL, as well as associated effects on the coherent electron dynamics. Near-field (NF) images (**Fig. 1f-g**) of monolayer (G1), bilayer (G2), and trilayer graphene (G3), and the corresponding graphene-WSe_2 heterostructures (W/G1, W/G2, W/G3) exhibit significant nanoscale heterogeneity not observed in far-field (FF) imaging. In addition, the FF and NF FWM responses differ with respect to their scaling with increasing graphene layer number as shown in **Fig. 1h**. Despite an appreciable FWM response from WSe_2 itself, we consistently observe a decrease in FWM intensity of the graphene-WSe_2 heterostructure compared to the FWM signals from corresponding homogeneous materials which suggests *interlayer coupling induces decoherence*. Moreover, a corresponding decrease in the WSe_2 2PPL signal with increasing graphene layer number suggests fast *interlayer-induced non-radiative quenching* that is further enhanced by the metallic tip-graphene pico-cavity.

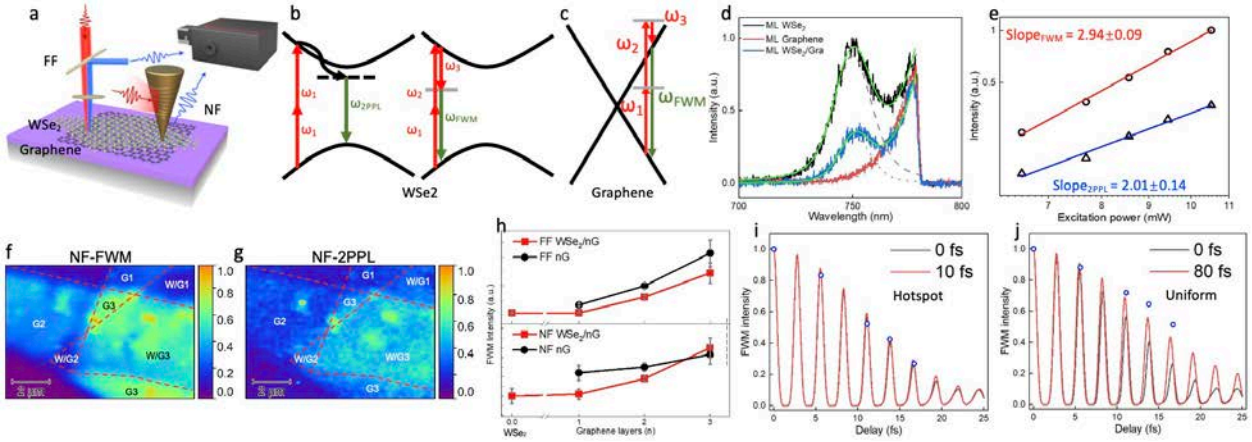

Fig. 1 (a) WSe_2/graphene nonlinear 2PPL and FWM nano-imaging, with corresponding pathways in WSe_2 and graphene (b,c). (d) Nano-2PPL and -FWM spectra in WSe_2, graphene, and their heterostructure. (e) Power dependence of 2PPL and FWM in monolayer WSe_2. (f-g) FWM and 2PPL images of the heterostructure. (h) Layer dependence of FWM intensities. (i-j) Coherence measurement of the inhomogeneous region (i) and homogenous region (j), showing a fast decoherence time of ~10 fs and a slower decoherence time of > 80 fs, respectively.

In addition, in FWM nano-imaging of monolayer WSe_2 itself, we observe distinct spatial heterogeneity with coherence times ranging from ~10 fs (**Fig. 1i**) in regions of high intensity to values exceeding 80 fs in regions with lower intensity (**Fig. 1j**). In contrast, our previous study of electronic coherence in monolayer graphene showed ultrafast dephasing of 6 ± 1 fs [4]. We interpret this counterintuitive effect as the result of defect scattering in localized states with higher nonlinear susceptibility yet faster dephasing time compared to structurally homogeneous WSe_2.

In summary, we correlate strong interlayer coupling, which gives rise to many of the unique excitonic and coherence properties of heterostructures, with nano-optical properties and their sensitivity to defects and heterogeneities. These findings are particularly significant for the development of optoelectronic devices relying on quantum coherence.

References

[1] M. A. May, et al. "Nanocavity clock spectroscopy: Resolving competing exciton dynamics in WSe_2/$MoSe_2$ heterobilayers," Nano Lett. **21**, 522 (2020).
[2] V. Kravtsov, et al. "Plasmonic nanofocused four-wave mixing for femtosecond near-field imaging," Nat. Nanotechnol. **11**, 459 (2016).
[3] V. Kravtsov, et al. "Enhanced third-order optical nonlinearity driven by surface-plasmon field gradients," Phys. Rev. Lett. **120**, 203903 (2018).
[4] T. Jiang, et al. "Ultrafast coherent nonlinear nanooptics and nanoimaging of graphene," Nat. Nanotechnol. **14**, 838 (2019).

Diffusion and lifetime of optical phase singularities

Thijs van Gogh[1], **Kobus Kuipers**[1]

1. Kavli Institute of Nanoscience Delft, Lorentzweg 1, 2628 CJ, Delft, The Netherlands

E-mail: m.a.vangogh@tudelft.nl

In general, the spatial structure of light fields contains exceptional points that exhibit singular behaviour. At these points, a parameter of the describing field becomes undefined, resulting in a distinct topology of the surrounding light field. Such singularities are ubiquitous in nature and occur in a plethora of systems, such as in black holes and at the bottom of a swimming pool. In light, these singularities can for instance manifest themselves as phase singularities, where the phase becomes undefined, or as points where the in-plane Poynting vector vanishes [1].

Random waves are arguably the most generic composition of a light field and their investigation yields insight in the basic behaviour of light itself. With our home-built phase- and polarization-resolving optical near-field microscope we experimentally study the temporal evolution of a random light field confined to 2D. We locate phase singularities in space and track their motion as a function of time. As they are topological in nature, they can only be created and annihilated in pairs of opposite topological charge. We can track their creation, movement and, ultimately, their annihilation in time and use concepts from statistical physics, such as the mean-square displacement, in order to study their diffusive properties. Additionally, the time-resolved data allows us to determine a mean lifetime of the singularities. We show that there is a significant difference in behaviour between *faithful* singularities -those that are annihilated with their birth partner-, and *unfaithful* singularities, which annihilate with a different partner. In Fig. 1a, we show the mean squared displacement for both faithful and unfaithful singularities. It is clear that unfaithful singularities diffuse further on average before being annihilated. In Fig. 1b we show the decay in population as a function of time. Again it is clear that unfaithful singularities live longer than their faithful counterpart. Furthermore, the decay shows a non-exponential decay for the faithful singularities, while the unfaithful ones show a decay that more closely resembles exponential decay.

Fig. 1 Differences between faithful (black dots) and unfaithful (red dots) singularities. (a) Shows the mean squared displacement (MSD) as a function of time. The unfaithful singularities consistently show a higher MSD than the faithful ones. (b) Shows the decline in population as a function of time. The unfaithful singularities show a much slower decline in population than the faithful ones.

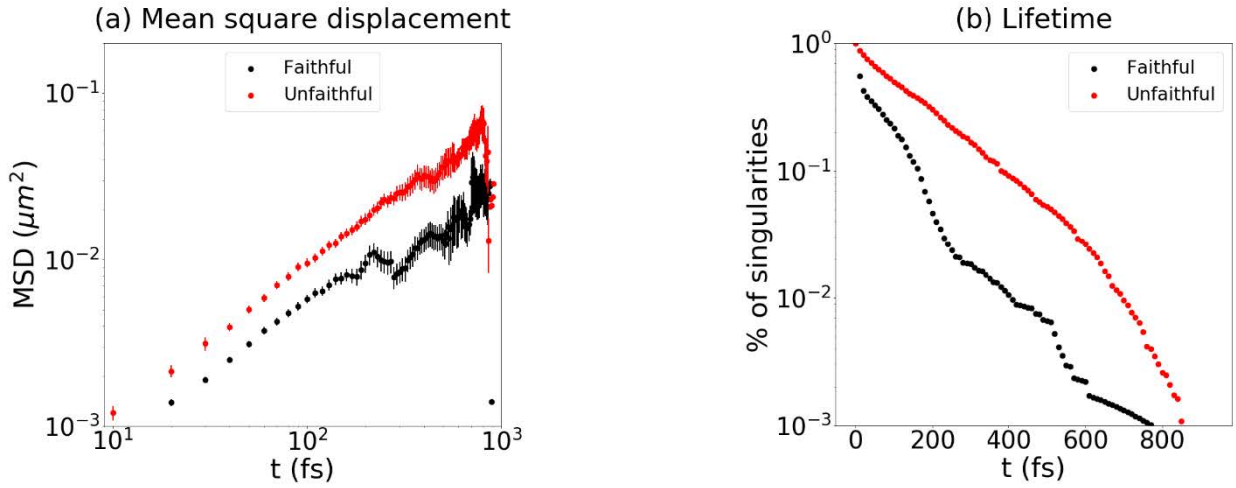

References

[1] Van Gogh, M.A., Bauer, T., De Angelis, L,. and Kuipers, L. 2020, *Opt. Lett.*, 45, 9: 2600-2603

Ultrafast electron probing of plasmon thermal dynamics

Eduardo Dias[1], **Vahagn Mkhitaryan**[1], **Javier García de Abajo**[1,2]

1. *ICFO - Institut de Ciencies Fotoniques, The Barcelona Institute of Science and Technology, 08860 Castelldefels (Barcelona), Spain*
2. *ICREA - Institució Catalana de Recerca i Estudis Avançats, Passeig Lluís Companys 23, 08010 Barcelona, Spain*

E-mail: eduardo.dias@icfo.eu

Thermal engineering of plasmons and other forms of polaritons in nanomaterials offers an appealing way of controlling light−matter interactions down to nanometer and femtosecond spatiotemporal scales. The study of ultrafast thermal dynamics traditionally relies on optical pump-probe experiments which are, however, limited in spatial resolution due to light diffraction. Electron energy-loss spectroscopy (EELS) performed on scanning transmission electron microscopes overcomes the optical diffraction limit by using electrons rather than light to map the material response with sub-Ångstrom spatial precision. In this work [1], we propose to study the ultrafast thermal dynamics of nanomaterials using an optical-pump/electron-probe (OPEP) technique with sub-Ångstrom and femtosecond spatiotemporal resolution.

Two-dimensional (2D) materials offer a splendid testbed for OPEP because they generally undergo substantial changes in their electronic structure under optical pumping. We start by applying this technique to highly doped self-standing graphene, which hosts electrically tunable plasmons. The graphene sample is optically pumped with an ultrafast laser (Figure 1a), which creates an elevated electronic temperature in the material that decays over a picosecond time scale. When probed with a delayed electron pulse, the graphene plasmon dispersion can be mapped out from the energy- and angle-resolved inelastically scattered electron distribution (Figure 1b,c). The dynamics of rapid heating and cooling of graphene electrons is traced through the delay-dependent variations observed in the distribution of scattered electrons.

We further show that the OPEP technique can be applied to doped graphene and undoped graphite ribbon samples. Interestingly, ribbons break translational invariance and produce lateral plasmon confinement, resulting in a discretization in electron deflection. Finally, we also show that the described excitations and their temporal dynamics can be revealed by integrating the inelastic electron signal over a broad energy range, thus avoiding the need for highly monochromatic electron beams and precise spectrometers.

This previously unexplored approach to study the ultrafast dynamics of optical excitations can be of interest to understand and manipulate polaritons in 2D semiconductors and other materials exhibiting a strong thermo-optical response.

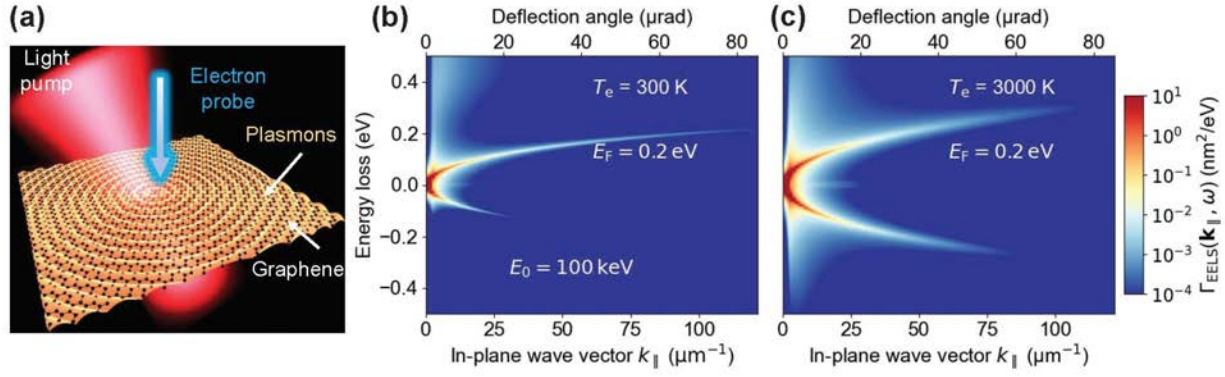

Fig. 1 OPEP characterization of plasmons in highly doped extended graphene. (a) Schematic representation of a graphene layer and OPEP configuration, with electrons impinging normal to the plane of the sample. (b, c) Momentum- and energy-resolved loss probability $\Gamma_{\mathrm{EELS}}(k_\parallel, \omega)$ for 100 keV transmitted electrons, revealing features associated with plasmon excitation in the sample for (b) low (300 K) and (c) high (3000 K) electronic temperature regimes. The graphene Fermi energy is $E_{\mathrm{F}} = 0.2$ eV and the intrinsic damping is $\hbar\tau^{-1} = 4$ meV.

References

[1] V. Mkhitaryan, E.J.C. Dias, F. Carbone, and F.J. García de Abajo, Ultrafast Momentum-Resolved Free-Electron Probing of Optically Pumped Plasmon Thermal Dynamics, ACS Photonics **8**, 614 (2021).

Phase mapping of the scattering signal from single plasmonic nanoparticles

Alfred J. Meixner*[1], Frank Wackenhut[1], Florian Laible[2], Monika Fleischer[2] and Kai Braun[1]

1. Institute of Physical and Theoretical Chemistry and Center LISA[+], University of Tuebingen, Auf der Morgenstelle 18, 72076 Tuebingen Germany
2. Institute for Applied Physics, University of Tuebingen and Center LISA[+], Auf der Morgenstelle 10, 72076 Tuebingen Germany
E-mail: alfred.meixner@uni-tuebingen.de

The interest in gold nanoparticles (GNPs) optical sensors is unbroken due to their unique optical properties which depend on their size, shape, and the interaction with their local chemical environment [1]. The distance dependent electronic coupling of dimers or trimers leads to a spectral shift of their resonance [2] and can be controlled by a DNA linker known as DNA-origami [3] or it is used to estimate nanoscale inter-particle, a concept known as plasmon ruler [4]. Single particle sensing is usually performed by recording white light spectra or luminescence spectra. The scattering cross section scales as the square of the particle volume and decreases drastically for small particles, also the luminescence quantum efficiency is low. An interesting alternative provides the interference of the elastically scattered signal with a strong reference which can easily be recorded by confocal interference microscopy [5]. For particles much smaller than the focal volume the signal collected by the objective is the sum of the elastically scattered background and the signal scattered by the particle and the contrast depends on their relative phase difference [6]. We have set out to investigate the phase of the scattered signal of individual GNPs with an inverted confocal microscope combined with a scanning Michelson interferometer and show that the phase shift caused by single gold nanorods with different aspect ratios can be reliably determined and related to shift of the particles plasmon resonance [7]. Furthermore we show that the phase change of the signal scattered of a dimer can be observed very sensitively when the gap distance is slightly changed [8]. Our work contributes to a better understanding of confocal scattering interference microscopy and provides new insight in single nanoparticle sensing.

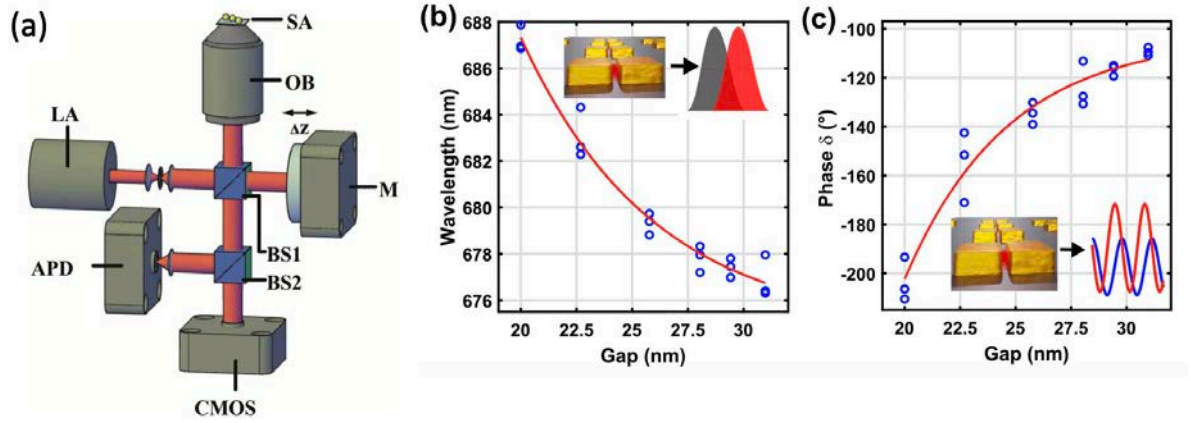

Fig. 1 (a) Confocal interference microscope to measure the phase scattered by a single gold nanoparticle. **(b, c)** Spectral shift of the luminescence maximum together with the respective phase shift of the elastically scattered signal as a function of the gap distance in a gold nanoparticle dimer.

References

[1] Link S, El-Sayed M A. 1999. *J Phys Chem B.* 103. 8410.
[2] Jain P K, El_Sayed M A. 2008. *J Phys Chem C.* 112, 4954.
[3] Dass M, Gür F N, Kołątaj K, Urban M J, Liedl T. 2021. *J Phys Chem* C. 125, 4969.
[4] Laible F, Horneber A, Fleischer M. 2021. *Adv Opt Mat.* 9, 2100126.
[5] Taylor R W, Sandogdar V. 2019. *NanoLett.* 19, 4827.
[6] Failla A V, Qian H, Hartschuh A, Meixner A J. 2006. *NanoLett.* 6, 1374.
[7] Hauler O, Wackenhut F, Jakob L A, Stuhl A, Laible F, et al. 2020. *Nanoscale*. 12, 1083.
[8] Hauler O, Jakob L A, Braun K, Laible F et al. 2021. *J Phys Chem C*. 125, 6486.

Quantitative Phase Imaging for Nanophotonics

Guillaume Baffou

Institut Fresnel, CNRS, Aix Marseille University, Centrale Marseille, Marseille, France

guillaume.baffou@fresnel.fr

Quadriwave lateral shearing interferometry (QLSI) is a quantitative phase microscopy technique that enables the mapping of the wavefront distortion of a light beam with both high spatial resolution and high sensitivity [1]. This contribution is aimed at explaining how QLSI can benefit the field of Nanophotonics, namely, (i) how QLSI can be used as a temperature microscopy technique to map the temperature of gold nanoparticles under illumination [2], enabling applications in physics [3], chemistry [4] and biology [5] at the nano/microscale; (ii) how QLSI can map the complex optical conductivity and complex refractive index of 2D materials [6] ; (iii) how QLSI can retrieve the complex optical polarizability of nanoparticles, along with the extinction, scattering and absorption cross section from a single interferogram image [7,8], and finally (iv) how QLSI can fully characterize metasurfaces.

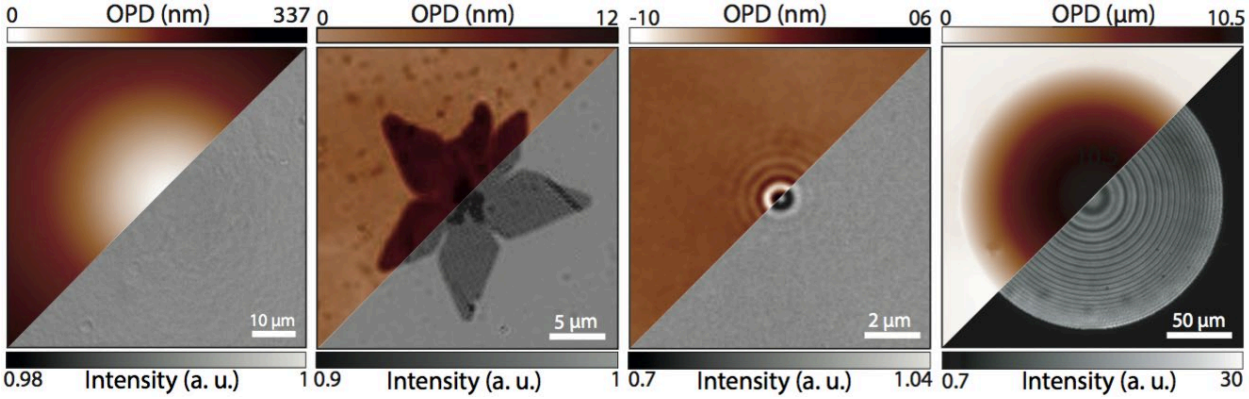

Fig. 1 Examples of intensity and optical-path-difference (OPD) images acquired using QLSI. From left to right: an assembly of gold nanoparticles under illumination, creating a localized, radial temperature gradient ; a MoS_2 flake ; a single 100-nm gold nanosphere and a metalens.

References

[1] Baffou, G. J. Phys D : Appl. Phys. J. Phys. D: Appl. Phys. 54, 294002 (2021)
[2] Baffou, G. ; Bon, P. ; Savatier, J. ; Polleux, J. ; Zhu, M. ; Merlin, M. ; Rigneault, H. ; Monneret, S. 2012. *ACS Nano* 6, 2452-2458
[3] Baffou, G. ; Berto, P. ; Bermúdez Ureña, E. ; Quidant, R. ; Monneret, S. ; Polleux, J. ; Rigneault , H. 2013. *ACS Nano* 7, 6478-6488 (2013)
[4] Robert, H. M. L. ; Kundrat, F. ; Bermudez-Urena, E. ; Rigneault, H. ; Monneret, S. ; Quidant, R. ; Polleux, J. ; Baffou, G. 2016. *ACS Omega* 1, 2-8
[5] Robert, H. M. L. ; Savatier, J. ; Vial, S. ; Verghese, J. ; Wattelier, B. ; Rigneault, H. ; Monneret, S. ; Polleux, J. ; Baffou, G. 2018. *Small* 14, 1801910
[6] Khadir, S. ; Bon, P. ; Vignaud, D. ; Galopin, E. ; McEvoy, N. ; McCloskey, D. ; Monneret, S. ; Baffou, G. 2017 *ACS Photonics* 4, 3130-3139 (2017)
[7] Khadir, S. ; Chaumet, P. ; Baffou, G. ; Sentenac, A. 2019. *J. Opt. Soc. Am. A* 36, 478-484
[8] Khadir, S. ; Andrén, D. ; Chaumet, P. C. ; Monneret, S. ; Bonod, N. ; Käll, M. ; Sentenac, A. ; Baffou, G. 2020. *Optica* 7, 243-248

Dielectric meta-optics for reconfigurable planar optics and biosensing

Romain Quidant[1]

1. *Nanophotonic Systems Laboratory, ETH Zurich, Zurich, Switzerland*

E-mail: rquidant@ethz.ch

In this talk, we present our latest advances in the development of novel nanophotonic platforms for both imaging and biosensing.

In the first part, we introduce our most recent advances in the development of reconfigurable planar optical elements, focusing on two original technologies. The first technology relies on dynamically controlling the distribution of refractive index by means of an engineered micro-resistor embedded in a thermo-optical material. We first show how our approach can be used to create varifocal lenses with 100ms response time. When combined with machine learning, this approach additionally enables to go beyond a simple lens and create complex phase fronts [1]. Our second approach to reconfigurability relies on an optomechanical control. Upon illumination with a control beam, the meta-atoms forming the lens mechanically rearrange, inducing a fast change of focus [2].

In the second part of the talk, we discuss the use of dielectric nanoresonators for biosensing and lab-on-a-chip technology. In our approach, Si nanoresonators are integrated into a state-of-the-art PDMS microfluidic environment. We first demonstrate that arrays of Si nanocylinders can be used for the specific detection of cancer markers in human serum with sensitivity levels comparable to the one obtained with gold nanoantennas. We also show how dielectric nanoresonators can benefit chiral molecular sensing, demonstrating enantio-selective differentiation with improved performance over plasmonics. Finally, we discuss different novel directions toward improved sensing performance and detection of emerging biomarkers [3].

References

[1] R. Steffen *et al*, submitted (2022)
[2] A. Afridi *et al*, submitted (2022)
[3] J. Garcia Guirado *et al*, submitted (2022)

Hyperbolic Meta-Antennas for Light-Matter Interaction Engineering

Sema Ebrahimi [1,2,3], Ali Adawi [2,3], Anne-Laure Baudrion [1], Pierre-Michel Adam [1], Jean-Sebastien Bouillard [2,3]

[1] Light, nanomaterials, nanotechnologies (L2n) Laboratory, CNRS EMR7004, University of Technology of Troyes, F-10004 Troyes Cedex, France

[2] Department of Physics and Mathematics, University of Hull, Cottingham Road, HU6 7RX, UK

[3] G.W.Gray Centre for Advanced Materials, University of Hull, Cottingham Road, HU6 7RX, UK

E-mail: sema.ebrahimi@utt.fr, s.ebrahimi-2019@hull.ac.uk

Hyperbolic Metamaterials are described as an emerging class of highly anisotropic plasmonic materials, providing electromagnetic properties on-demand. Based on their hyperbolic optical dispersion curves, hyperbolic metamaterials can support the propagation of high-k modes and represent a significant increase in the photonic density of states to engineer light-matter interactions [1, 2]. Here, we introduce a hyperbolic meta-antenna based on the multilayer Au/ TiO_2 bowtie nanostructures, supporting a type II hyperbolic dispersion. Effective medium theory (EMT) was used to calculate the effective index and optical responses of the hyperbolic meta-antennas.

We provide a detailed study of the physical mechanisms underlying the meta-antenna optical response. Using electric and magnetic field distributions, both in plane and out of plane, we identify two different modes supported by the multilayer antennas. We find that one mode is purely scattering while the other has a purely absorptive nature (Fig. 1b). The main scattering mode originates from the bonding electric dipolar modes between the two elements of the antenna (Fig. 1e), similar to the pure gold corresponding antenna (Fig. 1d). On the other hand, the absorptive mode at longer wavelengths is absent from the pure gold geometry and solely supported by the meta-antenna (Fig. 1f). Using the field distributions, we propose that this second mode arises from the excitation of magnetic dipolar modes in the meta-antenna.

Additionally, by tuning the metal filling factor in the meta-antenna multilayer system, we obtain full control over the intensity, spectral separation, and ratio of the scattering and absorption modes covering the visible and infrared regions (Fig. 1c). The proposed hyperbolic meta-antennas are highly promising for applications in optical sensors, sub-wavelength meta-cavity lasers, photocatalysis, and hot-electron generation processes.

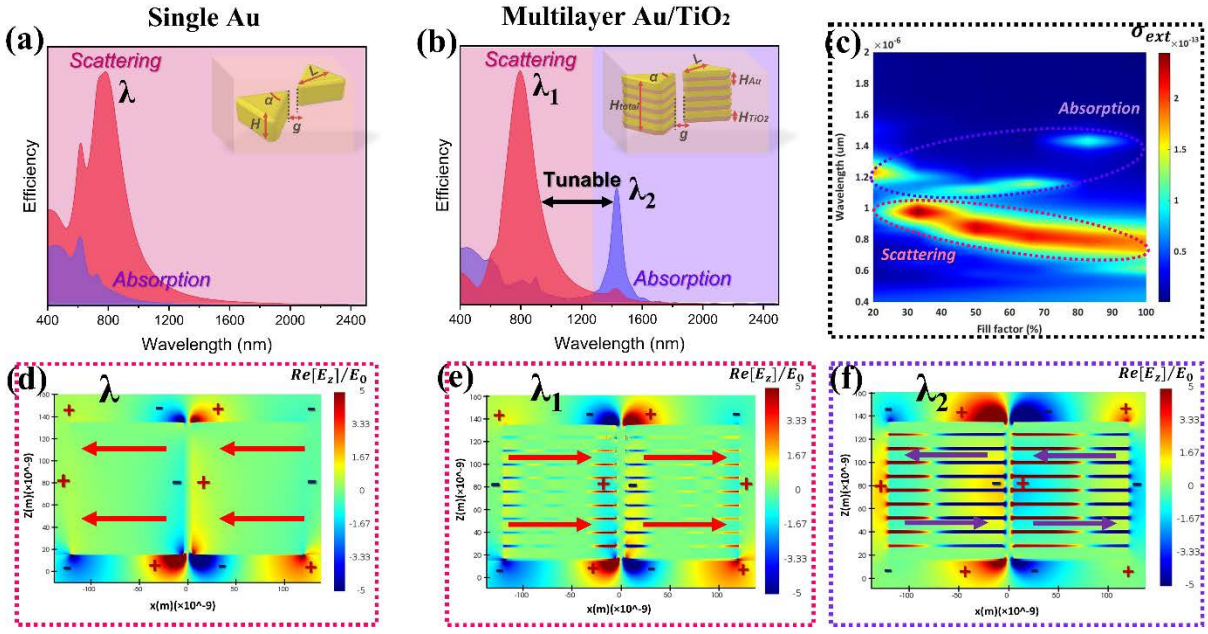

Fig. 1 Calculated Scattering and Absorption of (a) Single Au and (b) Multilayer Au/TiO_2 bowtie nanoantennas. (c) Tunability of the scattering and absorption modes as a function of fill factor of Au in the visible and infrared regions. Near-field distribution of the z-component of the electric field and related current density distributions of (d, e) the scattering and (f) absorption peaks related to the Single Au and multilayer Au/TiO_2 bowtie nanostructures, respectively.

References

[1] Poddubny, A., Iorsh, I., Belov, P., & Kivshar, Y. (2013). Hyperbolic metamaterials. Nature photonics, 7(12), 948-957.

[2] Maccaferri, N., Zhao, Y., Isoniemi, T., Iarossi, M., Parracino, A., Strangi, G., & De Angelis, F. (2019). Hyperbolic meta-antennas enable full control of scattering and absorption of light. Nano letters, 19(3), 1851-1859.

Enhanced fluorescence emission in nano-imprinted rare-earth-doped photonic metasurfaces

Michele Montanari[1,2], Zeinab Chehadi[3], Nicoletta Granchi[1,2], Mehrnaz Modaresialam[4], Mathieu Koudia[3], Mathieu Abel[3], Magali Putero[3], David Grosso[3,4], Francesca Intonti[1,2], Marco Abbarchi[3,4]

1. Department of Physics and Astronomy, University of Florence, Sesto Fiorentino 50019, Italy
2. LENS, University of Florence, Sesto Fiorentino 50019, Italy
3. Aix Marseille Univ, CNRS, Université de Toulon, IM2NP, UMR 7334, F-13397 Marseille, France
4. Solnil, Rue de la Republique, 13001 Marseille

E-mail: montanari@lens.unifi.it

Red light emission from Eu^{3+} doped phosphors is extensively used in lamp and display applications but the employment of such materials in thin film applications is hampered by their small absorption cross-section. However, by fabricating a suitable two-dimensional photonic crystal (PC) on top of a doped thin layer, the PC dispersion can be engineered to exhibit Bloch resonances spatially and spectrally tuned to the absorbing medium, and, by boosting both light absorption and light extraction, the luminescence can be greatly enhanced [1-3].

Here, we will review on the experimental and numerical investigation of square arrays of ZrO_2:Eu^{3+} nano-cylinders fabricated by soft nano-imprinting lithography on a fused silica substrate [4] (Fig.1 a)). This technique is advantageous for fast large-area production and for the fact that both the doped layer and the PC are realized with the same material at the same time without any other fabrication steps. Arrays with different periodicity *p* have been investigated using angle-resolved and angle-integrated measurements, supported by finite difference time domain (FDTD) simulations, to ensure the spectral and spatial coupling of Eu^{3+} emission with Bloch resonances (Fig. 1 b)). We experimentally demonstrate that, by varying *p*, we can modify the absorption of the excitation light and the outcoupling of the photoluminescence, achieving an enhancement of the luminescence intensity up to a factor ≈ 240 compared with the unpatterned flat surface (Fig. 1 c)) within the collection angle of a small numerical aperture lens (NA=0.28).

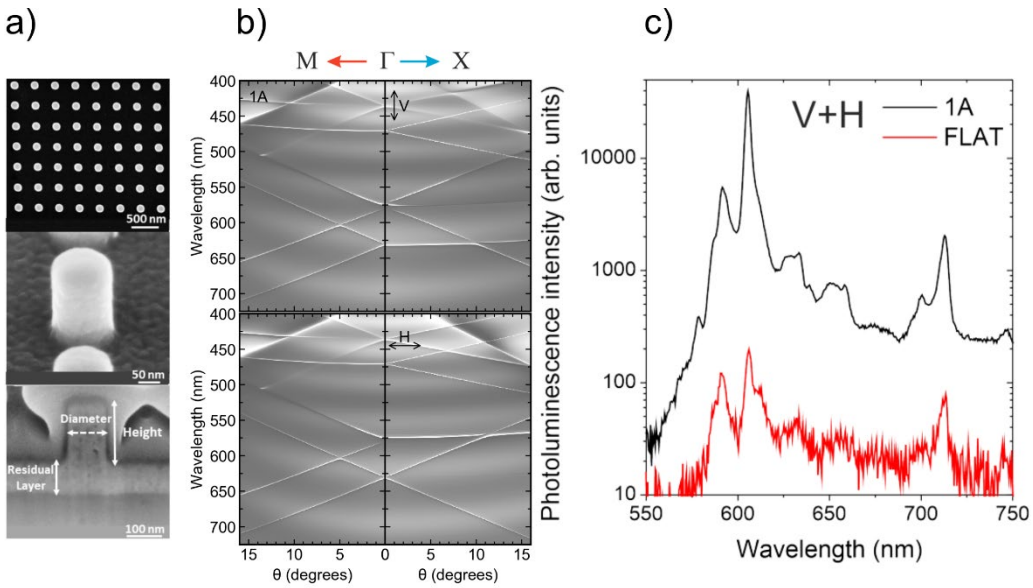

Fig. 1 a) Scanning electron microscopic (SEM) images of the ZrO_2:Eu^{3+} nanocylinder array at different magnifications. b) Theoretical simulations of the angle-resolved reflection of the metastucture (*p*=370 nm) along the Γ-M and Γ-X directions for two different polarizations of the incident light. c) Ange-integrated photoluminescence of the metastructure (*p*=370 nm, black curve) and of the unpatterned flat surface (red curve).

References

[1] Park, Y. et al., 2009, Opt. Express 17, 14312−14321.
[2] Noda, S. et al., 2007, Nat. Photonics, 1, 449−458.
[3] Hoang, N. V. et al., 2017, ACS Photonics 4, 1705–1712.
[4] Bottein, T. et al., 2018, Nanoscale 10, 1420–1431.

NFO16
Reconfigurable Hyperbolic Polaritonics with Correlated Oxide Metasurfaces

Yohannes Abate[1], Neda Alsadat Aghamiri[1], Guangwei Hu[2,3], Alireza Fali[1], Zhen Zhang[4], Jiahan Li[5], Sivacarendran Balendhran[6], Sumeet Walia[6,7], Sharath Sriram[7,8], James H. Edgar[5], Shriram Ramanathan[4], Andrea Alù[2,9]

1. Department of Physics and Astronomy, University of Georgia, Athens, Georgia 30602, USA
2. Photonics Initiative, Advanced Science Research Center, City University of New York, NY 10031, USA
3. Department of Electrical Eng., National University of Singapore, Kent Ridge, Singapore 117583, Singapore
4. School of Materials Engineering, Purdue University, West Lafayette, IN 47907, USA
5. Tim Taylor Department of Chemical Engineering, Kansas State University, Manhattan, KN 66506, USA
6. School of Engineering RMIT University Melbourne, Victoria, Australia
7. Functional Materials and Microsystems Research Group and the Micro Nano Research Facility RMIT University Melbourne, Australia
8. ARC Centre of Excellence for Transformative Meta-Optical Systems, RMIT University, Melbourne, Australia
9. Physics Program, Graduate Center, City University of New York, New York, NY 10016, USA

E-mail: Yohannes.abate@uga.edu

Polaritons enable subwavelength confinement and highly anisotropic flows of light over a wide spectral range, holding the promise for applications in modern nanophotonic and optoelectronic devices. However, to fully realize their practical application potential, facile methods enabling nanoscale active control of polaritons are needed. Here, we introduce a hybrid polaritonic-oxide heterostructure platform consisting of van der Waals crystals, such as hexagonal boron nitride (hBN) or alpha-phase molybdenum trioxide (α-MoO_3), transferred on nanoscale oxygen vacancy patterns on the surface of prototypical correlated perovskite oxide $SmNiO_3$ (SNO). Using a combination of scanning probe microscopy and infrared nanoimaging techniques, we demonstrate nanoscale real-time reconfigurability of complex hyperbolic phonon polaritons patterned at the nanoscale with unmatched resolution. Hydrogenation and temperature modulation allow spatially localized conductivity modulation of SNO nanoscale patterns, enabling robust real-time modulation and nanoscale reconfiguration of hyperbolic polaritons. Our work paves the way towards nanoscale programmable metasurface engineering as a new paradigm for reconfigurable nanophotonic applications facilitated by a hybrid material platform exploiting extreme light-matter interactions in polaritonic systems.

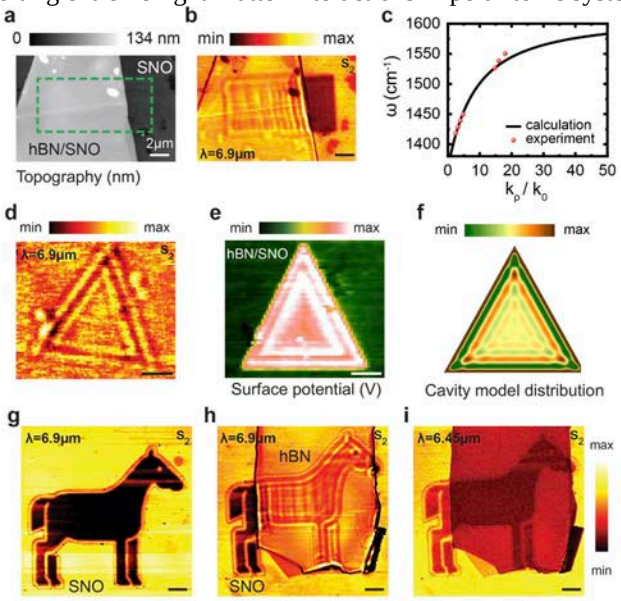

Fig. 1 | Tunable polaritonics with SNO-hBN architectures. a,Topographic image of pristine SNO, a lithography pattern is performed by applying 10 V potential at the c-AFM tip and a flake of 60 nm hBN (~99% boron-10 enriched) is transferred on top. **b**, IR s-SNOM second harmonic near field amplitude s_2 image. **c** Measurement of the dispersion relation of HPhPs in 60 nm thick hBN on SNO. **d**, Second-harmonic near-field amplitude s_2 image of a 60 nm hBN flake transferred on a triangular cavity lithographically patterned by applying a 10V potential c-AFM tip. **e** Corresponding KPFM surface potential images and **f**, simulation result (see Methods) for panel d. Second harmonic near field amplitude s_2 images of a lithographic pattern on SNO written by applying a 10V potential at c-AFM tip **g**, prior transferring a hBN flake and **h**, with a 50 nm thick hBN flake on top showing polaritons at 6.9 μm, and **i,** at 6.45 μm.

Plasmon-assisted lithium niobate metasurface with ultra-high-*Q* resonances

M. Saad Bin-Alam[1], M. Zahirul Alam[2], Ksenia Dolgaleva[1,2], and Robert W. Boyd[1,2,3]

[1]School of Electrical Engineering and Computer Science, University of Ottawa, Ottawa, ON, K1N 6N5, Canada
[2]Department of Physics, University of Ottawa, Ottawa, ON, K1N 6N5, Canada
[3]The Institute of Optics and Department of Physics and Astronomy, University of Rochester, Rochester, New York 14627, USA
E-mail: msaad009@uottawa.ca

Lithium niobate ($LiNbO_3$) is a material of choice in commercial implementations of second-order nonlinear optical devices [1-2]. Efficient $LiNbO_3$-based metasurfaces may lead to devices with new functionalities for free-space multimode applications such as mode-selective modulators, switches, beam shaping [3-5], *etc*. However, all nonlinear optical interactions scale with the propagation length and a sub-micron propagation distance typically does not afford strong-enough nonlinear interactions to realize high-efficient nonlinear devices [6]. Here we show that lattice-plasmons allows excitation of guided-mode resonances in $LiNbO_3$ thin films with quality factor (*Q*-factor) on the order of 10^4**.** Such high *Q* factors will allow efficient nonlinear interactions without phase matching concerns in a metasurface geometry.

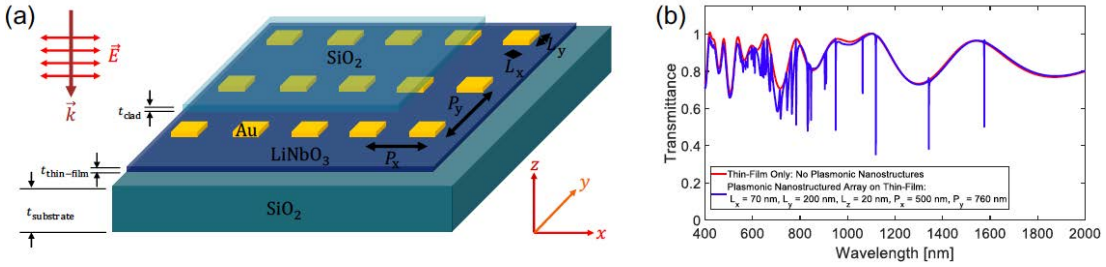

Fig. 1 (a) A schematic of a plasmonic metasurface on lithium niobate ($LiNbO_3$) thin film-on-insulator. The metasurface consists of a plasmonic gold (Au) antenna array placed on a high refractive-index thin-film with fused silica (SiO_2) substrate and cladding layers. (b) Comparison between the simulated broadband transmittance spectra with and without the plasmonic rectangular nanostructure array shown in (a).

A collection of periodic, plasmonic antennas with a certain periodicity or lattice constant operated as weak scatterers can direct normally incident light in various diffraction angles determined by the Bragg conditions [7-9]. When such a collection of antennas is placed on a sub-micron-thick film of $LiNbO_3$ (see Fig. 1(a)), they allow the excitation of many guided-wave modes (see Fig. 1(b)). Consequently, the transmission spectrum exhibits many comb-like resonance dips with *Q*-factors as large as 10^4 over an octave of visible and near-IR frequencies. We investigate the exact spectral location, the *Q*-factor, and nonlinear properties of the resonances as functions of the thickness of $LiNbO_3$, nature of the guided modes, and geometric properties of the plasmonic antennas (which dictates the radiative and nonradiative loss).

We believe that our demonstrations lay the groundwork for high-efficient nonlinear metasurfaces exploiting second-order nonlinear interactions.

References

[1] Saleh, B. E., Teich, M. C. *Fundamentals of Photonics*, 2019, John Wiley & Sons.
[2] Boyd, R. W. *Nonlinear Optics*, 2020, Academic Press.
[3] Weigand, H., Volgler-Neuling, V. V., Escalé, M. R., Pohl, D., Richter, F. U., Karvounis, A., Timpu, F., Grange, R. 2021. *ACS Photonics*, 8, 3004-3009.
[4] Klopfer, E., Dagli, S., Barton III, D., Lawrence, M., Dionne, J. A. 2022. *Nano Lett.*, Articles ASAP (In Press).
[5] Barton III, D., Lawrence, M., Dionne, J. 2021. *Appl. Phys. Lett*., 118, 071104.
[6] Fedotova, A., Younesi, M., Sautter, J., Vaskin, A., Löchner, F. J., Steinert, M., Geiss, R., Pertsch, T., Staude, I., Setzpfandt, F. 2020. *Nano Lett.*, 20, 8608−8614.
[7] Kravets, V. G., Kabashin, A. V., Barnes, W. L., Grigorenko, A. N. 2018. *Chem. Rev.*, 118, 5912-5951.
[8] Khlopin, D., Laux, F., Wardley, W.P., Martin, J., Wurtz, G.A., Plain, J., Bonod, N., Zayats, A.V., Dickson, W. and Gérard, D. 2017. *JOSA B*, 34, 691-700.
[9] Bin-Alam, M. S., Reshef, O., Mamchur, Y, Alam, M. Z., Carlow, G., Upham, J., Sullivan, B. T., Ménard, J-M, Huttunen, M. J., Boyd, R. W., Dolgaleva, K. 2021. *Nat. Commun.*, 12, 1-8.

Invited: Plasmonic Forces at the Picoscale

Jeremy Baumberg
NanoPhotonics Centre, Cavendish Laboratory, Department of Physics, University of Cambridge, United Kingdom
E-mail: jjb12@cam.ac.uk

For over 30 years, single molecule signatures in surface-enhanced Raman scattering (SERS) have suggested the extreme localisation of light, but the mechanisms involved remained elusive. Recently, this was finally explained as due to the light concentration around single metal adatoms on a plasmonically-active surface [1]. In strongly-confining nanocavities (constructed here from nanoparticle-on-mirror, NPoM, see Fig.1a), light is further confined on the sub-atomic scale by single atom asperities (Fig.1b) [1]. In this talk I will show how light is responsible for pulling out the Au or Ag atoms involved, and show different ways that this can be controlled.

We measure millions of SERS spectra from a wide range of NPoMs with different molecular monolayers forming their 1-2nm nanogaps, and automatically extract all picocavity events. We find a characteristic probability for formation, and for decay, which depends on light intensity, the molecule, and temperature. Traditional models based on classical optical forces from the field gradients completely fail to explain this data (Fig.1c), as they are thousand-fold too weak and would predict very long decay times. Instead we show a new effect is responsible, based on the light-induced van-der-Waals forces from plasmonically-enhanced dipole-dipole interactions arising via the polarizability of the tip atoms [2]. Shining light on a metal surface reduces the energy barrier required to pull out an atom from the facet.

Using two pump lasers simultaneously to track SERS from different spatial regions of the nanogaps allows lateral localisation of the picocavities produced [3]. It also confirms that picocavities have spectral resonances, and thus shows that they act as more than merely lightning rods. Using carboxylate molecules in the gap allows (de)protonation events at picocavities to be tracked in real time, for the first time giving optical measurements of pH at a single molecule [4]. We show that comprehensive analysis of picocavity SERS allows videos of individual molecules to be reconstructed [5]. Finally, we show that the optomechanical coupling of the vibrations with the plasmonic cavity allows efficient upconversion to detect mid-IR light [6].

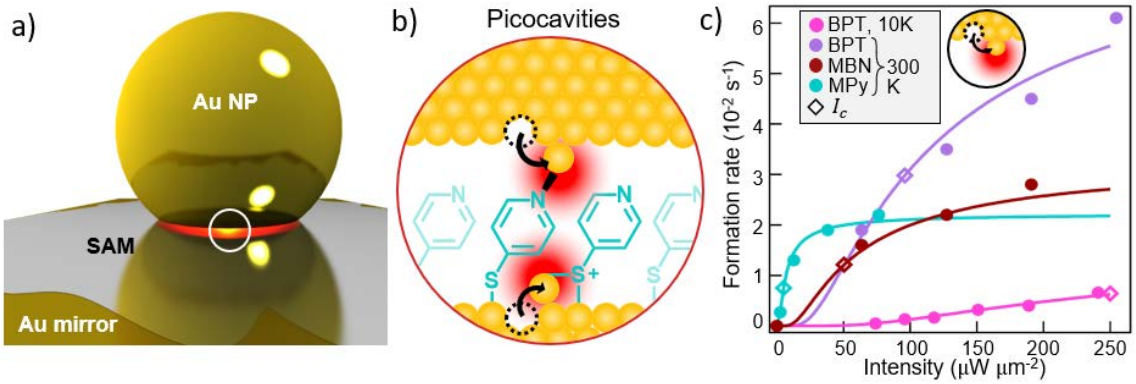

Fig. 1 (a,b) Nanoparticle-on-mirror cavity, trapping light in nanogap with molecules, which pull out adatoms to form picocavities. (**c**) Formation rate of picocavities depends on light intensity and molecule, on a universal curve.

These results are important in many areas, particular for photocatalysis but also for broad impacts in molecular (opto)electronics, biosensing, photovoltaics, and single-atom switches.

References

[1] F. Benz et al., "Single-molecule optomechanics in picocavities", Science **354**, 726 (2016)
[2] Q. Lin et al., "Optical suppression of energy barriers in single molecule-metal binding", submitted (2021)
[3] J. Griffiths et al., "Locating Single-Atom Optical Picocavities ...", ACS Photonics **8**, 2868 (2021)
[4] J. Huang et al., "Tracking interfacial single-molecule pH and binding dynamics ...", Science Advances **7**:eabg1790 (2021)
[5] J. Griffiths et al, "Resolving sub-Å ambient motion through reconstructions from vibrational spectra", Nature Comm **12**:6759 (2021)
[6] A Xomalis et al, Detecting mid-IR light by molecular frequency upconversion in dual-wavelength nanoantennas, Science **374**, 1268 (2021)

Optical mode imaging via correlated free-electron cavity-photon pairs

Germaine Arend[1,2], **Armin Feist**[1,2], **Guanhao Huang**[3], **Yujia Yang**[3], **Jan-Wilke Henke**[1,2], **Arslan Sajid Raja**[3], **F. Jasmin Kappert**[1,2], **Jiahe Pan**[3], **Hugo Lourenco-Martins**[1,2], **Zheru Qiu**[3], **Junqiu Liu**[3], **Ofer Kfir**[1,2], **Tobias J. Kippenberg**[3], **Claus Ropers**[1,2]

1. 4th Physical Institute, University of Göttingen, Friedrich-Hund-Platz 1, D-37077 Göttingen
2. Max-Planck Institut for Multidisciplinary Sciences, Am Fassberg 11, D-37077 Göttingen
3. Swiss Federal Institute of Technology Lausanne (EPFL), CH-1015 Lausanne, Switzerland

E-mail: germaine.arend@uni-goettingen.de

Free electrons and photons are widely used as probes in atomic-scale imaging and high-resolution spectroscopy, respectively. Applying electron microscopy to optical excitations is a powerful approach harnessing spontaneous electron energy-loss and cathodoluminescence imaging [1], as well as stimulated near-field scattering [2]. Bringing the inelastic electron-light interaction to the single-particle regime will open up new pathways for free-electron quantum optics, including electron-photon entanglement [3]. This, however, requires the enhancement of the typically weak coupling between free electrons and photonic modes.

Here, we establish fiber-coupled, photonic-chip-based silicon nitride microresonators as a versatile platform for inducing efficient coupling between free electrons and light [4]. Inelastic scattering of electrons at the vacuum states of the microresonator leads to a quantized electron energy loss and correlated cavity photon generation.

Scanning the focussed electron beam, passing parallel to the chip surface, maps the interaction with the optical resonator mode. The transmitted electrons are analysed in energy and arrival time using an event-based detector (cf. Fig 1a). Simultaneously, the generated photons are detected with a fiber-coupled single-photon avalanche diode (SPAD), time-tagging each single-electron event. Correlating the arrival times of the two particles, a coincidence peak at 0.8-eV electron energy loss (cf. Fig 1b) is observed, revealing the generation of electron-photon pairs. Filtering the events using energy loss and time delay enables the exclusive study of the correlated particles. The resonator modes are imaged by mapping the photon generation rate for variable electron beam position (Fig 1d, top). Spectral filtering to a single mode leads to Ramsey-type interferences [5] at the empty cavity (Fig 1d, bot), as also observed for stimulated scattering at an externally pumped resonator (cf. Fig 1c) [4]. Finally, we demonstrate a strong contrast enhancement in imaging of the photonic mode by using correlated events only.

In summary, we demonstrate the efficient coupling of single free electrons and cavity photons by inelastic electron-light scattering, which enables high-fidelity heralded single-electron or single-photon sources. This promises novel experimental concepts, including the controlled generation of photon Fock states, as well as coincidence-enhanced photonic mode imaging.

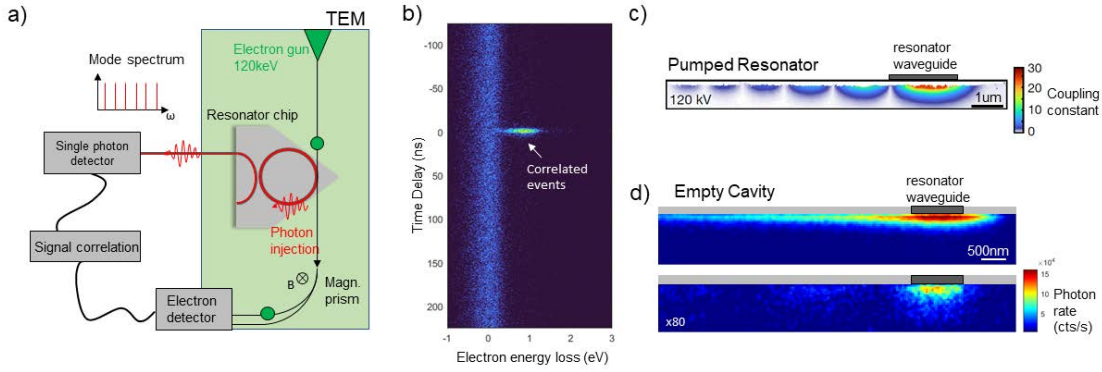

Fig. 1 (a) Schematic experimental setup and photon generation process, introducing a fiber-coupled high-Q microresonator in a transmission electron microscope; (b) Detected electrons as a function of energy loss and relative time delay to the nearest photon, revealing a pronounced correlation peak; (c) electron-light coupling constant measured via stimulated electron scattering at an optically pumped resonator (reproduced from [4]); (d) Rate of detected photons as a function of electron beam position along the resonator using the full optical spectrum (top) and filtering to a single mode (bottom).

References

[1] Polman, A., Kociak, M., Garcia de Abajo, F.J.. 2019. *Nature Mat* 18 1158-1171
[2] Barwick, B., Flannigan, D.J., Zewail, A.H.. 2009. *Nature* 462 902-906
[3] Kfir, O.. 2019. *Phys. Rev. Lett.* 123, 103602
[4] Henke, J.-W. et al.. 2021. *Nature* 521 200-203
[5] Echternkamp, K. et al.. 2016. *Nature Phys* 12 1000-1004

Sub-diffractional cavity modes of terahertz hyperbolic phonon polaritons in tin oxide nanobelts

Flávio H. Feres [1,2,9], Rafael A. Mayer[1,2,9], Lukas Wehmeier[3,4], Francisco C. B. Maia[1], E. R. Viana[5], Angelo Malachias[6], Hans A. Bechtel[7], J. Michael Klopf[8], Lukas M. Eng[3,4], Susanne C. Kehr[3], J. C. González[6], Raul O. Freitas[1] & Ingrid D. Barcelos[1]

1 Brazilian Synchrotron Light Laboratory (LNLS), Brazilian Center for Research in Energy and Materials (CNPEM), Campinas, SP, Brazil.

2 Physics Department, Gleb Wataghin Physics Institute, University of Campinas (Unicamp), Campinas, SP, Brazil.

3 Institute of Applied Physics, Technische Universit t Dresden, Dresden, Germany.

4 ct.qmat, Dresden-Würzburg Cluster of Excellence-EXC 2147, Technische Universit t Dresden, Dresden, Germany.

5 Department of Physics, Universidade Tecnológica Federal do Paraná (UTFPR), Curitiba, PR, Brazil.

6 Department of Physics, Universidade Federal de Minas Gerais (UFMG), Belo Horizonte, MG, Brazil.

7 Advanced Light Source (ALS), Lawrence Berkeley National Laboratory, Berkeley, CA, USA.

8 Institute of Radiation Physics, Helmholtz-Zentrum Dresden-Rossendorf, Dresden, Germany.

E-mail: raul.freitas@lnls.br

In the last few years, hyperbolic phonon polaritons have attracted considerable attention in nanophotonics mostly due to their intrinsic strong electromagnetic field confinement, ultraslow polariton group velocities, and long lifetimes. Here we present tin oxide (SnO_2) nanobelts as a photonic platform for the transport of mid to far-IR surface and volume phonon polaritons. This communication brings a comprehensive description of the polaritonic properties of SnO_2 as a nanometer-sized dielectric and as an engineered material in the form of a waveguide. By combining accelerator-based IR-THz sources (synchrotron and free-electron laser) with s-SNOM, we employed nanoscale far-infrared hyperspectral-imaging to uncover a Fabry–Perot cavity mechanism in SnO_2 nanobelts via direct detection of phonon-polariton standing waves. Our experimental findings are accurately supported by notable convergence between theory and numerical simulations. After the publication of these results [1], SnO_2 is now confirmed as a natural hyperbolic material with unique photonic properties essential for future applications involving subdiffractional light traffic and detection in the far-infrared range.

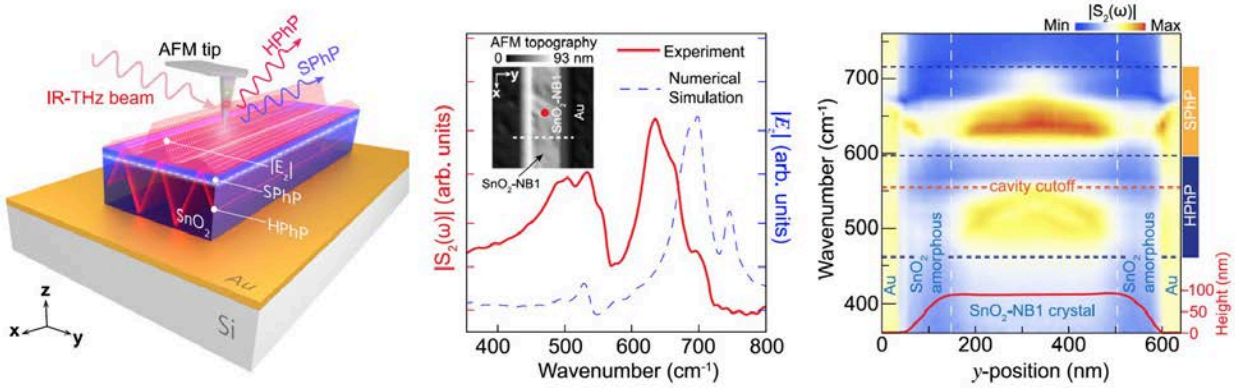

Fig. 1 (*left*) Experimental schematic showing the IR-THz beam illuminating a metallic AFM tip (nano-antenna) for the s-SNOM experiment. The highly confined and vertically polarized electric fields (Ez) at the tip apex launch surface (SPhPs) and volume (HPhPs) polaritons waves in the SnO_2-NB. (*center*) SINS amplitude $S_2(\omega)$ point spectrum (red solid line) of the SnO_2-NB1. Inset shows 1x1 μm^2 AFM topography of the SnO_2-NB1 (t = 93 nm, w = 350 nm), and the red dot indicates the SINS point spectrum location. FDTD-simulated spectrum (blue dashed line) obtained from |Ez| integration along out-of-plane axis. (*right*) SINS spectral linescan along the white-dashed line in the inset in (center). Figure adapted from [1].

References

[1] F. H. Feres, R. A. Mayer, L. Wehmeier, F. C. B. Maia, E. R. Viana, A. Malachias, H. A. Bechtel, J. M. Klopf, L. M. Eng, S. C. Kehr, J. C. González, R. O. Freitas, I. D. Barcelos, *Nature Communications* **12**, 1995 (2021).

Real-space nanoimaging of THz polaritons in the topological insulator Bi_2Se_3

Shu Chen[1], Andrei Bylinkin[1,2], Zhengtianye Wang[3], Martin Schnell[1,4], Greeshma Chandan[3], Peining Li[5], Alexey Y. Nikitin[2,4], Stephanie Law[3], Rainer Hillenbrand[4,6]

1. CIC nanoGUNE BRTA, 20018 Donostia - San Sebastián, Spain
2. Donostia International Physics Center (DIPC), 20018 Donostia - San Sebastián, Spain
3. IKERBASQUE, Basque Foundation for Science, 48009 Bilbao, Spain
4. Wuhan National Laboratory for Optoelectronics & School of Optical and Electronic Information, Huazhong University of Science and Technology, Wuhan 430074, China
5. Department of Materials Science and Engineering, University of Delaware, Newark, Delaware, 19716 USA
6. CIC nanoGUNE BRTA and Department of Electricity and Electronics, UPV/EHU, 20018 Donostia-San Sebastián, Spain

E-mail: r.hillenbrand@nanogune.eu

Plasmon polaritons in van der Waals materials and topological insulators (TI) attract attention from a fundamental perspective and for potential THz photonic applications. Although polaritons have been observed by THz far-field spectroscopy on topological insulator microstructures, real-space imaging of propagating THz polaritons has been elusive so far. Here, we show spectroscopic THz near-field images of thin Bi_2Se_3 layers (prototypical topological insulators) revealing polaritons with up to 12 times increased momenta as compared to photons of the same energy and decay times of about 0.48 ps, yet short propagation lengths.

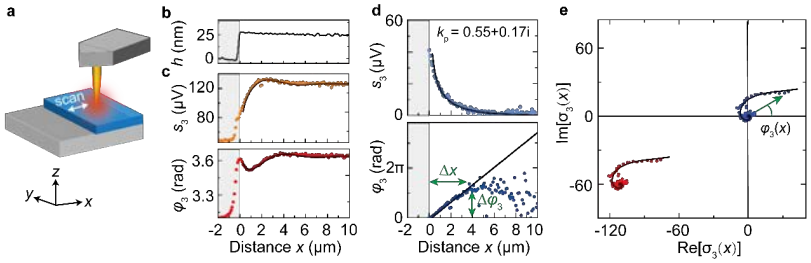

Fig. 1 Complex-valued analysis of THz near-field line profiles of a 25 nm thick Bi_2Se_3 film. a Sketch of s-SNOM experiment. **b** Topography line profile, showing the height *h* as measured by AFM. **c** Experimental s-SNOM amplitude and phase line profiles recorded at 2.52 THz. **d** Amplitude and phase line profiles obtained from the data shown in panel c after subtraction of the complex-valued signal offset *C* at large distances *x*. **e** Representation of near-field line profiles in the complex plane. Data corresponding to panel c are shown in red colour, data corresponding to panel d are shown in blue colour**. c-e** The black solid lines show the fitting of the experimental data by a radially and exponentially decaying wave.

We recorded real-space images of THz polaritons in the TI Bi_2Se_3. Despite the short polariton propagation, we could measure the polariton dispersion and propagation length, owing to complex-valued analysis of near-field line profiles, which we will discuss in detail (Fig. 1). The highly specific signature of polaritonic spatial signal oscillations in the complex plane – representing a spiral – could be also applied in the future to distinguish polaritons from non-polaritonic spatial signal oscillations that, for example, are caused by spatial variations of dielectric material properties or by laser intensity fluctuations.

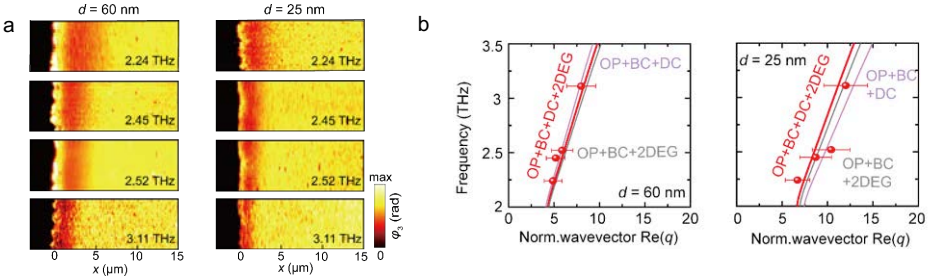

Fig. 2 Polaritons in Bi_2Se_3 films with *d* = 60 nm and 25 nm thickness. **a** Near-field phase images at different THz frequencies. **b** Polariton dispersions. Red symbols in the diagrams show the polariton dispersions obtained by complex-valued fitting of experimental line profiles as demonstrated in Fig. 1. Solid lines show calculated dispersions based on various conductivity models. We consider various optical conductivity contributions based on optical bulk phonons (OP), massive bulk carriers (BC), Dirac carriers (DC) at both Bi_2Se_3 surfaces, and massive two-dimensional electron gases (2DEG) at both Bi_2Se_3 surfaces.

Using dispersion calculations based on various optical conductivity models (Fig. 2), we found that the polaritons in Bi_2Se_3 can be explained by simultaneous coupling of THz radiation to various combination of Dirac carriers, massive 2DEG carriers, massive bulk carriers and optical phonons. Our work paves the way for studying THz polaritons in various conducting thin layers, as we will show with further examples including thin semiconductor layers.

References

[1] S. Chen et al., arXiv:2107.10791

Tunable second harmonic generation in plasmonic nanogaps by local symmetry breaking

Jessica Meier[1], **Luka Zurak**[1], **Andrea Locatelli**[2], **René Kullock**[1], **Thorsten Feichtner**[1], **Bert Hecht**[1]

1. Nano-Optics and Biophotonics Group, Experimental Physics 5, University of Würzburg, Germany
2. Department of Information Engineering, University of Brescia, Italy
E-mail: jessica.meier@physik.uni-wuerzburg.de

Plasmonic nanostructures exhibit large field enhancement which is commonly exploited to boost nonlinear optical effects such as second harmonic (SH) generation [1]. Especially intense near-field hot spots emerge in the gap of dimer antennas upon excitation of their antisymmetric (bonding) mode. For antennas with a centrosymmetric shape, however, the strong SH sources created at the vicinal metal surfaces in the gap region oscillate out-of-phase and thus destructively interfere in the farfield [2].

Here, we demonstrate that it is possible to systematically tune the SH yield by breaking the mirror symmetry in the gap region while retaining the overall antisymmetric resonance at the fundamental frequency. To this end, we employ gallium- and helium-ion beam milling of single-crystalline gold microplatelets [3], which allows us to top-down fabricate nanostructures at a precision down to three nanometers. Due to the advanced control over the geometric and thus optical properties of the antennas, we are able to compare the SH yield of asymmetric antennas featuring only one tip with their respective symmetric counterparts (Fig. 1). For asymmetric antennas, SH intensity increases dramatically with smaller tip opening angles corresponding to a higher degree of asymmetry, whereas only a weak increase of SH intensity is observed for symmetric antennas. Our experimental results are supported by full nonlinear simulations using a frequency-domain finite element method. The quantitative agreement between experiment and simulation further confirms the high accuracy and reliability of our fabrication approach and corroborates the underlying theoretical description.

Our results provide the basis for future experiments that will introduce further tunability of the SH response and will make use of multiresonant structures and improved materials to optimize the SH efficiency.

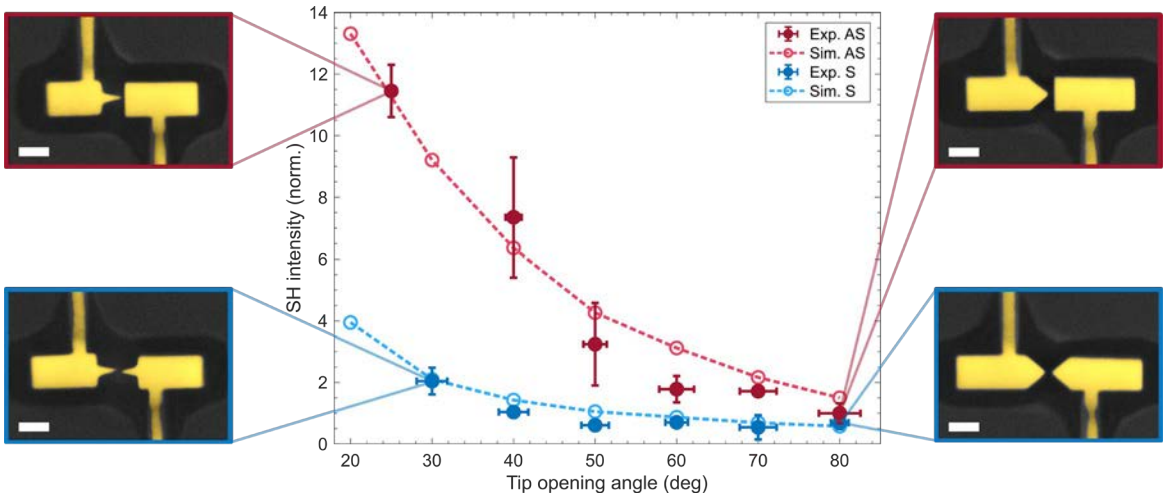

Fig. 1 Measured and simulated SH intensity from asymmetric (red) and symmetric (blue) optical antennas dependent on the tip opening angle. Error bars account for measurements on different antennas with comparable geometric and linear optical properties. Scanning electron micrographs show antennas with smallest (left) and largest (right) tip opening angle. Scale bars, 50 nm.

References

[1] Celebrano, M., Wu, X., Baselli, M., Großmann, S., Biagioni, P., Locatelli, A., De Angelis, C., Cerullo, G., Osellame, R., Hecht, B., Duò, L., Ciccacci, F., Finazzi, M. 2015. *Nature Nanotech*, 10, 412-417.
[2] Berthelot, J., Bachelier, G., Song, M., Rai, P., Colas des Francs, G., Dereux, A., Bouhelier, A. 2012. *Opt. Express*, 20, 10498-10508.
[3] Krauss, E., Kullock, R., Wu, X., Geisler, P., Lundt, N., Kamp, M., Hecht, B. 2018. *Cryst. Growth Des.*, 18, 1297-1302.

Near-arbitrary spectral placement of lattice resonances using Fourier analysis

Theng-Loo Lim[1], **Yaswant Vaddi**[1], **M. Saad Bin-Alam**[2], **Lin Cheng**[3], **Rasoul Alaee**[1], **Jeremy Upham**[1], **Ksenia Dolgaleva**[2], **Orad Reshef**[2], **Robert W. Boyd**[1,2,4]

1. Department of Physics, University of Ottawa, 25 Templeton St, Ottawa, ON, K1N 6N5, Canada.
2. School of Electrical Engineering and Computer Science, University of Ottawa, 25 Templeton St, Ottawa, ON, K1N 6N5, Canada.
3. School of Instrument and Electronics, North University of China, Taiyuan, 030000, China.
4. Institute of Optics and Department of Physics and Astronomy, University of Rochester, 500 Wilson Blvd., Rochester, New York, 14627, USA

E-mail: tlim103@uottawa.ca

Resonances in optical systems are useful for many applications, such as frequency comb generation [1] and biosensing [2]. However, many of these applications are difficult to implement in optical metasurfaces because traditional approaches for designing multi-resonant nanostructures require significant computational and fabrication efforts. To address this challenge, we introduce Fourier lattice resonance (FLR) design technique, in which simply knowing the desired multiple resonances is sufficient to determine the metasurface structure [3]. Because each resonance is supported by a distinct surface lattice mode, each can have a high-quality factor [4]. This flexible procedure requires only the computation of a single Fourier transform for its design and then require only standard lithographic fabrication methods, allowing one to design and fabricate a metasurface to fit any specific, optical-cavity-based application.

To demonstrate the FLRs concept, we first select a set of desired resonance wavelengths and create a virtual spectrum (Fig. 1a), where we deliberately place two SLRs at 1150 nm and 1220 nm. We label this set of desired wavelengths as FLR1. Then, we extend the spectrum by adding replicas of these two desired resonances at integer harmonics in this virtual spectrum (i.e., $\lambda_{SLR}/2$, $\lambda_{SLR}/3$, *etc*.) for which higher-order diffraction terms will naturally appear for any lattice resonance. We then take the inverse FT (IFT) of the virtual spectrum (Fig. 1b), producing a series of peaks in the spatial domain that indicate the nanoparticle particle positions necessary to produce surface lattice resonances at the desired wavelengths. We calculate the transmission spectra of this IFT-generated lattice arrangement using the lattice sum approach (LSA) [5] and confirm peaks at the desired positions (Fig. 2 c, blue). We repeat this approach with another set of desired wavelengths (1310 nm and 1550 nm, FLR2, Fig 1c red), and again producing the desired transmission spectrum.

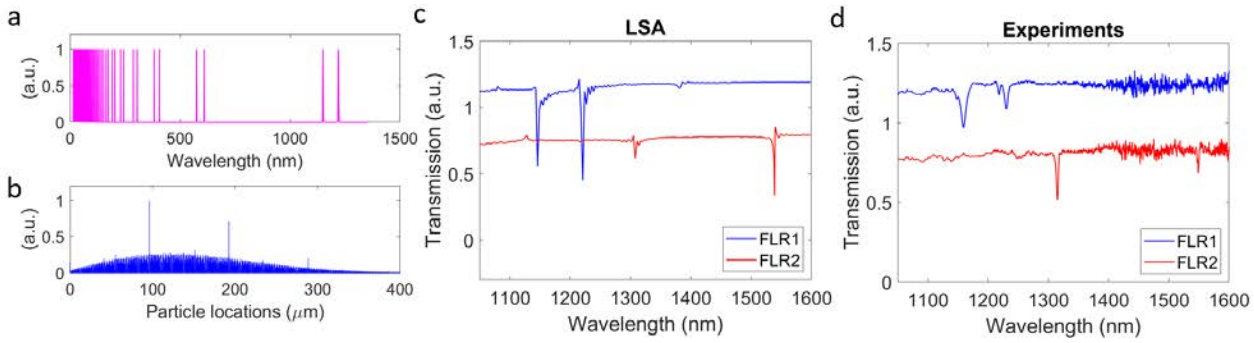

Fig. 1 The demonstration of Fourier lattice resonance (FLR) concept. (a) The generated virtual spectrum. (b) The Fourier transform (FT) of the virtual spectrum. (c) The calculated transmission spectra of two set of lattice arrangements, labelled as FLR1 and FLR2, using the FT-simulated particle spacing and lattice sum approach (LSA). (d) The experimental transmission spectra of FLR1 and FLR2.

To experimentally verify the FLR method, we fabricated these metasurfaces consisting of rectangular particles, and their corresponding spacings according to the IFT-generated lattice arrangements. Their experimentally characterized transmission spectra (Fig. 1d) confirm the desired resonances are obtained by the FLR technique. Because this approach can easily generate metasurface solutions from only the desired spectra, it could provide designs for applications with spectra too complex to fully simulate otherwise and may reveal insight into how these SLR can be still further engineered.

References

[1] Okawachi, Yoshitomo, et al. 2011. Opt. Lett 36.17, 3398-3400.
[2] Menezes, Jacson W., et al. 2010. Adv. Funct. Mater 20.22, 3918-3924.
[3] Lim, Theng-Loo, et al. 2021. arXiv preprint arXiv:2112.11625.
[4] Bin-Alam, M. Saad, et al. 2021. Nat. Commun, 12.1: 1-8.
[5] Draine, Bruce T., and Piotr J. Flatau. 1994. J. Opt. Soc. Am. A 11.4, 1491-1499.

Efficient Coupling of Visible Light into a Plasmonic Slit Waveguide

Marc Noordam[1], **Kobus Kuipers**[1]

1. *Kavli Institute of Nanoscience Delft, Department of Quantum Nanoscience, Delft University of Technology, Lorentzweg 1*

E-mail: m.l.noordam@tudelft.nl

Confining guided light modes into dimensions below the diffraction limit has been one of the most interesting challenges of the nanophotonic research community. Plasmonic waveguides are very promising for guiding light below the diffraction limit, some recent demonstrations include the coupling of a plasmonic waveguide mode to an excitonic mode in a few-layer transition metal dichalcogenide (TMDC) material [1] and nonlinear harmonic generation along a plasmonic gold nanowire [2].

However, plasmonic waveguides, especially in the visible regime, suffer from two major challenges. Firstly, plasmonic modes typically suffer from high losses in the metallic structure leading to short propagation lengths. Secondly, the typically large wavevector mismatch between free-space light and the plasmonic mode gives rise to a low coupling efficiency. An effective coupling mechanism should therefore ideally adiabatically transform a dielectric light mode into a plasmonic mode over relatively short length scale, to prevent large losses during the coupling.

Following a concept for telecom frequencies [3], here we demonstrate a nanofabricated device converting a dielectric mode at visible frequencies into a plasmonic slit waveguide mode. A sketch of the intersection of our device can be observed in fig. 1(a,b). A thin layer of silicon nitride is encapsulated in silicon dioxide where two gold plates with a small gap in between are placed on top. When the gap between the metallic plates is large enough the mode is mainly confined in the silicon nitride waveguide while as the gap closes the mode can be adiabatically transferred into the plasmonic slit mode. For the visible frequency regime silicon does not work as a dielectric layer and another dielectric material must be used. Since only the even plasmonic mode couples to the dielectric mode and the even mode increases when the gap closes, the dielectric mode can only couple into the plasmonic mode if its effective index is larger than that of the plasmonic mode at large gap width. Therefore, we extensively simulate this hybrid model to find the precise device parameters that can transform the dielectric mode to the even plasmonic mode in the visible frequencies. The resulting simulated effective index of the hybrid mode as function of the gap width is plotted in fig. 1(c).

Figure 1(d) depicts a scanning electron microscope image of our fabricated coupling device where we use a specially designed high index silicon nitride layer. Here, a diffraction grating is used to couple incoming free-space light into the silicon nitride. Next, the silicon nitride light mode is adiabatically coupled to the slit plasmon mode by reducing the gap between the gold plates. After propagation through the slit the plasmon mode is similarly coupled back to free-space light. We are currently preforming optical experiments to explore the transmission as a function of the slit width and length.

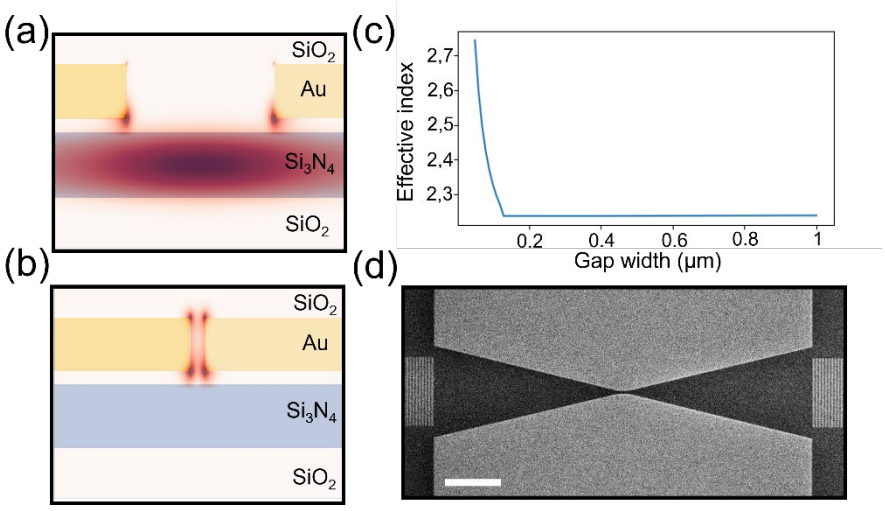

Fig. 1 (a,b) Schematic representation of the mode coupler for slit opening widths of 1 μm (a) and 100 nm (b). The simulated local electric field distribution of the corresponding hybrid mode is overlayed as a false-color map. (c) The simulated effective refractive index of the hybrid mode as a function of the slit opening width. (d) Scanning electron microscope image of a fabricated hybrid coupling device, scale bar is 5 μm.

References

[1] Gong, S. H., et al., 2018, *Science,* 359.6374, 443-447.

[2] de Hoogh, A., et al., 2016, ACS Photonics, 3.8: 1446–1452

[3] Nielsen, Michael P., et al. 2016. *Nano Lett,* 16.2, 1410-1414.

Nanoscale photodetectors based on graphene and graphene nanoribbons for integrated plasmonic circuitry

Mo Lu[1], Seyed Khalil Alavi[1], Boris V. Senkovskiy[2], Dirk Hertel[1], Danny Haberer[3], Yoichi Ando[2], Klaus Meerholz[1], Felix R. Fischer[3,4,5], Alexander Grüneis[2], and Klas Lindfors[1]

1. Department für Chemie, Universität zu Köln, Greinstr. 4-6, 50939 Köln, Germany
2. II. Physikalisches Institut, Universität zu Köln, Zülpicher Strasse 77, 50937 Köln, Germany
3. Department of Chemistry, University of California at Berkeley, 699 Tan Hall, Berkeley, CA 94720, USA
4. Materials Sciences Division, Lawrence Berkeley National Laboratory, Berkeley, CA 94720, USA
5. Kavli Energy NanoSciences Institute at the University of California Berkeley and the Lawrence Berkeley National Laboratory, Berkeley, California 94720, USA

E-mail: klas.lindfors@uni-koeln.de

Transmitting optical signals between a distant nanoscale transmitter and receiver in a wireless optical link could enable low-loss large-distance communication between nano-objects [1,2]. For practical signal transmission a key requirement is the conversion between electrical and optical signals at the transmitter and receiver in the link. In this contribution we present our progress in realizing integrated plasmonic circuitry making use of nanoscale photodetectors based on graphene and graphene nanoribbons.

Armchair edge graphene nanoribbons (AGNRs) with tunable bandgap are a promising material for electronics and optoelectronics. We have earlier investigated the photophysical properties of seven atom wide AGNRs (7-AGNRs) [3, 4]. A particularly interesting feature of GNRs is their high absorption compared to graphene, which is beneficial for photodetection. We have recently demonstrated a nanoscale photodetector based on 7-AGNRs [5]. Figure 1 shows an electron micrograph of the device, which consists of a set of finger electrodes fabricated on top of a layer of aligned 7-AGNRs. Absorption of light results in photogenerated carriers in the semiconducting ribbons, which are transported between the source and drain electrodes under a bias voltage. The responsivity of the detector at a wavelength of 635 nm is 0.04 mA/W and the dark current is below 30 pA for a bias voltage of 1.5 V. The aligned ribbons result in a highly polarization dependent responsivity: Only light polarized along the ribbons is absorbed efficiently.

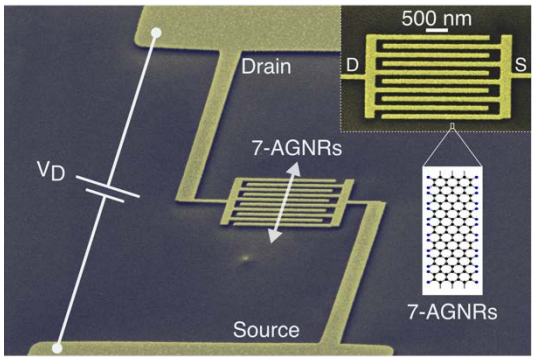

Fig. 1 Scanning electron micrograph of photodetector based on 7-AGNRs. The arrow shows the orientation of the GNRs.

In addition to 7-AGNR-based photodetectors, we have explored devices with graphene as the active material. In such a detector the photogenerated carriers near electrodes can be harvested due to band-bending near the metal-graphene interface [6]. By incorporating plasmonic nanoantennas into the structure, the absorption efficiency can be engineered and locally enhanced. In combination with a nanoscale transmitter, we have taken the first steps to realize wireless signal transmission using plasmonically enhanced graphene photodetectors.

Our simple proof-of-concept experiments highlight the promise of graphene-based photodetectors for integrated plasmonic circuitry. In particular graphene nanoribbons offer a flexible material platform with engineerable material properties making them a highly interesting option for nanoscale photodetectors. Graphene nanoribbons have the potential of being a key material for future optoelectronics and electronics.

References

[1] Alù, A.; Engheta, N. 2010. *Phys. Rev. Lett.*, 104, 213902.
[2] Dregekely, D.; Lindfors, K.; Lippitz, M.; Engheta, N.; Totzeck, M.; Giessen, H. 2014. *Nature Communications*, 5, 4354.
[3] Senkovskiy, B. V.; Pfeiffer, M.; Alavi, S. K.; *et al.* 2017. *Nano Lett.*, 17, 4029–4037.
[4] Alavi, S. K., *et al.* 2019. *2D Materials*, 6, 035009.
[5] Alavi, S. K., *et al.* 2020. *ACS Appl. Nano Mater.*, 3, 8343–8351.
[6] Liu, Y., *et al.* 2011. *Nature Communications*, 2, 579.

Atomistic Near-Field Optics

V. Ara Apkarian
Department of Chemistry, University of California at Irvine, Irvine, CA 92697, USA
aapkaria@uci.edu

The pursuit of ever increasing resolution has driven the major advances in the long history of microscopy. From the perspective of interrogating molecular matter, resolving atoms would be the sought natural limit, which in optical microscopy has been attained through tip-enhanced Raman scattering (TERS) carried out in the atomistic near-field (ANF) [1-4]. The essential concept dates back to Synge's proposal of near-field optics [5,6] to break the diffraction limit $d{\sim}\lambda_0/2n$ established by Abbe [7] and Helmholtz [8]. The modern solution is to use a plasmonic lens, $Re(n^2) \equiv \varepsilon' < 0$, to focus light, following the seminal works of Takahara and Nerkararyan, who pointed out that there is no cut-off for light guided on a 1D wire [9], a 2D wedge [10] or 3D cone [11] structures of negative dielectric. On a conical structure, since the index of refraction scales as the inverse cone radius $n \propto 1/r$, classically, there is no limit to focusing of light [11]. In practice, the classical singularity of the cone at $r = 0$ is eliminated by the atomic granularity (quantization) of matter, which explains the demonstrations of atomically confined light at the end of an atomically terminated silver needle [1-4]. While the description of the photon on a needle, namely the quantized electromagnetic displacement, is readily obtained by solving the 1D scaled heterogeneous Helmholtz equation (SHHE), $\nabla^2 + n^2(r) = 0$, the implications are far-reaching. Quantization of the displacement, of entangled light field and polarization of matter, $D = \varepsilon E = E + 4\pi P$, most naturally arises by the quantization of the dielectric, given by the eigenvalues of the SHHE. The associated eigenmodes nicely describe the antenna, waveguide, and super-focusing functionalities of a tapered plasmonic wire, as a paradigm that generalizes from TERS to SERS at plasmonic junctions. Notably, the apex mode on atomic asperities is atomically confined, which explains the physical volume of picocavities [12]. However, due to the dramatic increase in the dielectric $n^2 = (c/v_F)^2$, it consists entirely of polarization: the photon is self-trapped as it adiabatically converts to charge density $e\delta n$ and acquires mass $\sqrt{\varepsilon - 1}\hbar\omega/c^2$ consistent with the relativistic wave equations. With regard to microscopy, ANF optics can be just as well regarded as near field scanning tunneling electron microscopy (STEM), which is demonstrated experimentally by approach curves that characterize the tunneling conductance of the plasmon-polariton. Among the exciting applications of ANF optics is electro-photonics accessed by direct wiring of photons to intramolecular circuitry. More fundamentally, the extreme confinement forces rethinking of paradoxes that arise in quantization of relativistic wave equations, required to describe a photon in deep sub-wavelength plasmonic structures.

References

[1] Crampton, K. T., Lee, J., Apkarian, V. A. 2019. *ACS Nano 13, 6363.*
[2] Lee, J ., Crampton, K. T., Tallarida, N., Apkarian, V. A. 2019. *Nature 568, 7750*.
[3] Lee, J., Tallarida, N., Chen, X., Jensen, L., Apkarian, V. A. 2018. *Science Advances 4, eaat5472*.
[4] Tallarida, N., Lee, J., Apkarian, V. A. 2017. *ACS Nano 11, 11393*.
[5] Synge, E. H. 1928. *Phil. Mag. 6, 356-362*.
[6] Synge, E. H. 1932. *Phil. Mag. S7, 13, 297-300*.
[7] Abbe, E. 1873. Archiv. F. *Mikroskop. Anat, 9, 413*.
[8] Helmholtz, H. 1874. *Annal. Phys. 557-584*.
[9] Tkahara, J., Yamagishi, S., Taki, H., Morimoto, A., Kobayashi, T. 1997. *Optics Lett. 7, 475*.
[10] Nerkararyan, Kh., V. 1997. *Phys. Lett. A, 237, 103*.
[11] Babadjanian, A. J., Margaryan, N. L., Nerkararyan, Kh., V. 2000. *J. Appl. Phys. 87, 3785*.
[12] Urbieta, M., Barby. M. Zhang, Y., Koval, P., Sánchez-Portal, D., Zabala, N., Aizpurua, J. 2008. *ACS Nano, 12, 585*.

Advanced hybrid plasmonic nano-emitters using smart photopolymer

Dandan Ge[1], Ali Issa[1], Safi Jradi[1], Christophe Couteau[1], Sylvie Marguet[2] and Renaud Bachelot[1]

1. Light, nanomaterials, nanotechnologies (L2n) Laboratory. CNRS EMR 7004. Université de Technologie de Troyes, 12 rue Marie Curie, 10004 Troyes Cedex, France
2. CEA, CNRS, NIMBE, Université Paris Saclay, F-91191 Gif sur Yvette, France
E-mail: renaud.bachelot@utt.fr

The integration of quantum emitters onto plasmonic nano-devices with spatial control and nanometer precision has become a great challenge, e. g. [1-6].

We report on the use of a smart polymer for selectively immobilizing nano-emitters on specific preselected sites of gold nanocubes (GNC). The cunning use of the polymer is twofold. First, it records both the selected site and the future emitters-GNC distance through plasmon-assisted photopolymerization [5-6]. Second, because the polymer is chemically functionalized [7], it makes it possible to attach the nano-emitters right at the preselected polymerized sites which subsequently "recognize" the nano-emitters to get attached.

Since the resulting active medium is a spatial memory of specific plasmonic modes, it is anisotropic, making the hybrid nanosources sensitive to light polarization.

By controlling the thickness of the nanopolymer, the ability to adjust the statistical average photoluminescence lifetime of the hybrid emitters is demonstrated on two kinds of nano-emitters coupled to GNC: doped polystyrene nanospheres and semiconductor colloidal quantum dots.

Fig. 1 shows an example of hybrid nano-emitter with CdSe/ZnS Quantum Dots (emitting at 623 nm) that were integrated onto the surface of a functionalized polymer that has been patterned through plasmonic photopolymerization.

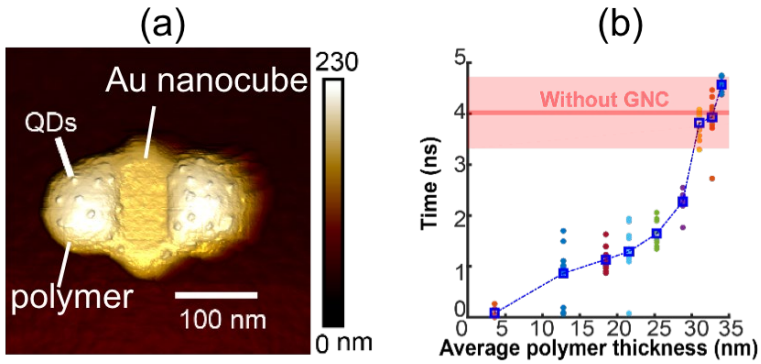

Fig. 1 Use of the smart polymer for coupling spherical CdSe/ZnS quantum dots with a gold nanocube. (a) AFM image of the hybrid nanosource. Attached QDs are clearly visible. (b) Weighted photoluminescence lifetime (λ=620 nm) as a function of the average polymer thickness that depends on the fabrication condition.

References

[1] Russell, K. J. et al. 2012. *Nature Photon.,* 6, 459-462.
[2] Ming, T. et al. 2009. *Nano Lett.*, 9, 3896–3903.
[3] Schell, A. W. et al. 2014. *Nano Lett.*, 14, 2623–2627.
[4] Hübner, K. et al. 2019. *Nano Lett.,* 19, 6629–6634.
[5] Ge, D. et al. 2020. *Nat. Commun.,* 11, 3414, 2020.
[6] Zhou, X. et al. 2015, *Nano Lett.*, 15, 7458–7466.
[7] Issa, A. et al. 2021. *ACS Appl. Mater. Interfaces*, 13, 41846–41856.

Nonlinear plasmonic response in atomically thin metal films

A. Rodríguez Echarri[1], **Joel D. Cox**[2,3] **and F. Javier García de Abajo**[1,4]

1. ICFO – Institut de ciències fotòniques, The Barcelona Institute of Science and Technology, 08860 Castelldefels, Barcelona, Spain

2. Center for Nano Optics, University of Southern Denmark, Campusvej 55, DK-5230 Odense M, Denmark

3. Danish Institute for Advanced Study, University of Southern Denmark, Campusvej 55, DK-5230 Odense M, Denmark

4. ICREA – Institució Catalana de Recerca i Estudis Avançats, Passeig Lluís Companys 23, 08010 Barcelona, Spain

arodriguez@icfo.net

Crystalline metallic films are attracting significant attention within the nanophotonics community as a material platform for plasmonics that offers light concentration and manipulation on extreme subwavelength scales with lower intrinsic losses than for plasmons in amorphous metal films [1,2]. Recent advances in nanotechnology now enable the fabrication of such crystalline films with nanometer-scale thickness, down to the level of only several atomic monolayers, further boosting plasmon confinement for the miniaturization of next-generation electronic and photonic devices. However, in very thin crystalline metallic films, quantum mechanical effects play a non-negligible role in the dynamics of electrons and their interaction with external electromagnetic fields, manifesting in the spectral features associated with its linear optical response that depend on film thickness and crystallographic orientation. These effects are anticipated to become even more significant when dealing with nonlinear optical phenomena, which necessitate intense optical fields that access additional transitions among quantized electronic states.

Here we reveal quantum and finite-size effects in the nonlinear optical response associated with plasmons supported by few-atom-thick crystalline noble metal films (see Fig 1a) [3]. In particular, we employ a quantum-mechanical description that captures the main features in the electronic band structure associated with the various crystal facets of noble metals [4] to simulate their nonlinear optical response by extending the random-phase approximation to higher orders. Our results demonstrate strong signatures of film thickness and crystallographic orientation in the linear plasmonic response that are amplified in nonlinear optical processes such as harmonic generation and two-photon absorption (see Fig. 1e), with additional effects attributed to surface states, electron spill out, and the directional band gap associated with bulk atomic-layer corrugation (see Fig c-d). These findings are of key importance in the characterization of atomically-thin crystalline films and their applications for nonlinear plasmonic nanophotonic devices.

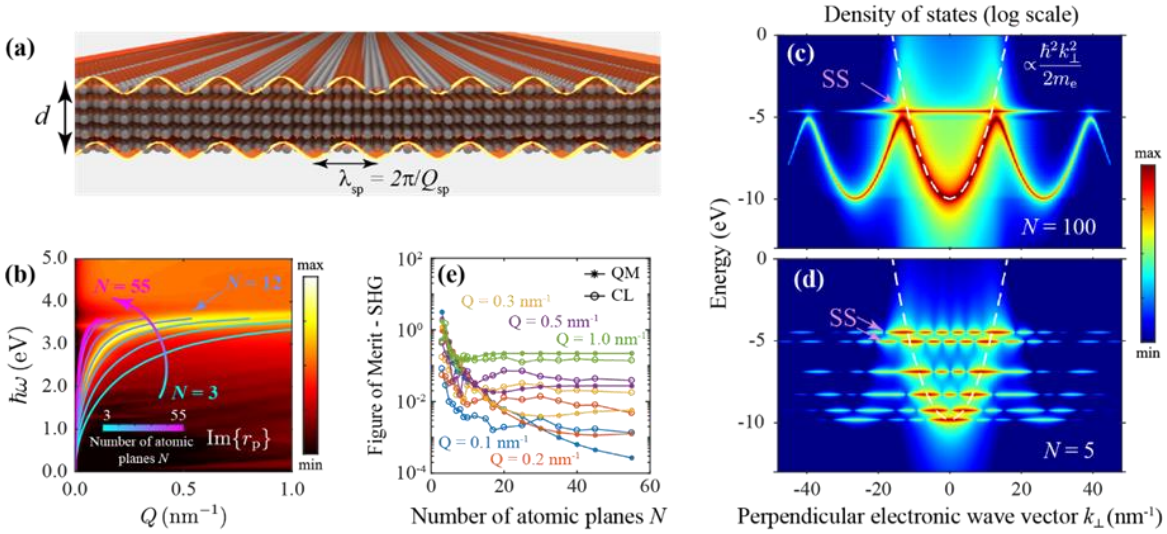

Fig. 1: (a) Illustration of surface plasmons (SP) in a few-atom-thick silver (111) film. (b) SP dispersion relation calculated via the loss function (imaginary part of the reflection coefficient) in momentum and energy space. Dispersion curves of SPs for various thicknesses are superimposed on the dispersion map and indicated by the colored code in the legend. (c,d) Electronic density of states obtained by Fourier-transforming the out-of-plane electronic wave functions for $N = 100$ and $N = 5$ Ag(111) atomic layers, respectively. (e) Figure of merit quantifying the nonlinear plasmonic yield using quantum-mechanical (filled circles) or classical (hollow circles) models for selected values of the in-plane wave vector Q.

References

[1] D. N. Basov, M. M. Fogler and F. J. García de Abajo. Science **354**, aag1992 (2016).
[2] D. Alcaraz Iranzo et al., Science **360**, 291 (2018).
[3] A. Rodríguez Echarri, J. D. Cox, and F. J. García de Abajo, Optica **6**, 630 (2019).
[4] E. V. Chulkov, V. M. Silkin and P. M. Echenique, Surf. Sci. **437**, 330 (1999).

Surface-response functions and their role in emitter—plasmon coupling

Christos Tserkezis[1], **Fedor A. Shuklin**[1], **Vasilios Karanikolas**[2], **Ioannis Thanopulos**[3], **P. André D. Gonçalves**[1], **Takashi Kuroda**[4], **Jun-ichi Inoue**[4], **Masakazu Ichikawa**[5], **Emmanuel Paspalakis**[3], **Christian Wolff**[1], **Joel D. Cox**[1,6], **and N. Asger Mortensen**[1,6]

1. Center for Nano Optics, University of Southern Denmark, Campusvej 55, DK-5230 Odense M, Denmark
2. International Center for Young Scientists, National Institute for Materials Science, 1-1 Namiki, Tsukuba, Ibaraki 305-0044, Japan
3. Materials Science Department, School of Natural Sciences, University of Patras, Patras 265 04, Greece
4. National Institute for Materials Science, 1-1 Namiki, Tsukuba, Ibaraki 305-0044, Japan
5. Department of Applied Physics, Graduate School of Engineering, The University of Tokyo, Bunkyo-ku, Tokyo 113-8656, Japan
6. Danish Institute for Advanced Study, University of Southern Denmark, Campusvej 55, DK-5230 Odense M, Denmark

ct@mci.sdu.dk

Surface-response functions (SRFs), in the spirit of the work of Feibelman [1], have been emerging as an efficient approach for implementing quantum corrections in the description of metals for nanoscale light—matter interactions. This appeal is owed to their ability to capture effects such us nonlocal screening, electron spill-in or spill-out, and surface-enabled Landau damping [2], which cannot be disregarded when considering plasmonic nanoparticles (NPs) of less than ~10 nm sizes, or separations smaller than ~2 nm. But the aforementioned separations do not necessarily refer to the particle—particle distance; they can equally well concern the distance between a plasmonic system and a quantum emitter. Coupling to localised surface plasmons in small NPs provides an excellent mechanism for tailoring the excitation and emission properties of such emitters, leading to significantly modified decay rates and the possibility of strong coupling [3]. It is thus reasonable to expect that quantum effects will play a major role in the plasmon—emitter interaction, and the implementation of SRFs in the theoretical description of this interaction should shed light on the phenomena governing the coupling.

SRFs are typically calculated with *ab initio* quantum methods for solid-state physics that take the full electron dynamics into account [1,2]. Here we show that much of the underlying quantum response can already be captured in the context of the local response approximation, by just relaxing its usual step-function approximation for the electron density *n* at the metal—dielectric interface, and assuming a smoothly varying density profile instead [4] (Fig. 1a). Once these functions have been obtained, they can be implemented in any otherwise classical model for computational electrodynamics, by simply appropriately modifying the boundary conditions [5]. At a next step, we form a metal—dielectric—metal cavity, with the metal described by actual calculated SRFs, and place a quantum emitter in the middle (Fig. 1b, top sketch). We show that the inclusion of quantum corrections in the response of the metal through SRFs not only does not prevent the system from entering the strong coupling regime, but it can, in fact, lead to interesting non-Markovian relaxation dynamics for the emitter [6] (Fig. 1b, bottom graph). We thus establish SRFs as a viable and computationally efficient way to consider aspects of the microscopic response of the metal in studying emitter—plasmon coupling.

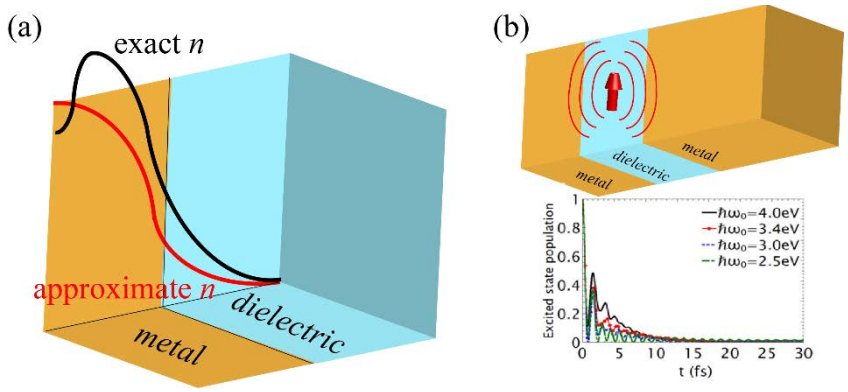

Fig. 1 (a) Schematic of a metal—dielectric interface with a sketch of an exact electron density (black line) and the approximation used in [4] (red line). (b) A metal—dielectric—metal cavity with a dipolar emitter in the middle (top). For different emitter transition energies the system undergoes various interesting dynamics (bottom),

References

[1] Feibelman, P. J. 1982. *Prog. Surf. Sci.*, 12, 287-407.
[2] Mortensen, N. A. 2021. *Nanophotonics*, 10, 2563-2616.
[3] Novotny, L. and Hecht, B. *Principles of Nano-Optics*. 2006, Cambridge University Press, Cambridge U.K.
[4] Mortensen, N. A., Gonçalves, P. A. D., Shuklin, F. A., Cox. J. D., Tserkezis, C., Ichikawa, M, and Wolff, C. 2021. *Nanophotonics*, 10, 3647-3657.
[5] Gonçalves, P. A. D, Christensen, T., Rivera, N., Jauho, A.-P., Mortensen, N. A., and Soljačić, M. 2020. *Nat. Commun.*, 11, 366.
[6] Karanikolas, V., Thanopulos, I., Cox, J. D., Kuroda, T. Inoue J.-I., Mortensen, N. A., Paspalakis, E., and Tserkezis, C. 2021. *Phys. Rev. B*, 104, L201405.

Quantum purity of entangled states of light scattered by a nanostructure

Álvaro Nodar[1], **Ruben Esteban**[1,2], **Carlos Maciel-Escudero**[1,3] , **Jon Lasa-Alonso**[1,2], **Javier Aizpurua**[1,2] , and **Gabriel Molina-Terriza**[1,2,3]

1. Centro de Física de Materiales CFM (CSIC-UPV/EHU), Paseo Manuel de Lardizabal, 5, 20018, Donostia, Spain
2. Donostia International Physics Center DIPC, Paseo Manuel de Lardizabal, 4, 20018, Donostia, Spain
3. CIC NanoGUNE BRTA and Dept. of Electricity and Electronics UPV/EHU, Avda. Tolosa, 76, 20018, Donostia, Spain
4. IKERBASQUE, Basque Foundation for Science, Calle María Diaz de Haro, 48013, Bilbao, Spain

E-mail: alvaro_nodar001@ehu.eus

Quantum states of light are excellent carriers of quantum information, as they are very robust to propagation decoherence. Furthermore, exploiting the angular momentum properties of these states makes it possible to encode more information and increase their robustness to decoherence. Interestingly, nanostructures designed to enhance light-matter interaction can enable the manipulation at the nanoscale of the quantum information. However, practical applications usually require that the purity of the quantum states is preserved in the interaction with the nanoparticle.

In this work, we provide a theoretical framework to analyze the preservation or destruction of the quantum purity of quantum states of light scattered by a nanostructure. Within this framework we first calculate the classical response of nanostructures illuminated by beams with well-defined angular momentum [1, 2]. This calculation gives the input parameters for a quantum description of the scattering process based on the quantum lossy beam splitter formalism [3]. We apply this methodology to a system of experimental relevance [4], the scattering by a rotationally symmetric nanostructure of two-photons states entangled in angular momentum. Specifically, we consider the input pulsed state $|\Psi_+^{in}\rangle = \phi(\omega_0, t_0)\,[|+\rangle|+\rangle + |-\rangle|-\rangle]$, where ϕ is the Gaussian envelope (with central frequency ω_0 and time t_0), and $|+\rangle$ and $|-\rangle$ describe photons states with helicity $\Lambda = +1$ and $\Lambda = -1$, respectively (Λ is the spin projected in the direction of propagation). The rotational symmetry of the nanostructure enables excellent control of the scattered state because it imposes the conservation of the total angular momentum. However, we find that the scattering of $|\Psi_+^{in}\rangle$ can lead to the loss of purity of the output state (see Fig. 1b) which can help understand recent experimental results [4].

We show that the loss of purity is due to the excitation of two (or more) optical resonances of the nanostructure that are spectrally sharp. The exact calculations are complemented with an analytical expression that connects the loss of purity with the optical response of the nanoscatterer. This expression is obtained by using a simplified physical picture that describes the output state as a superposition of two pulsed states that are time-delayed and frequency-shifted due to the scattering by the nanostructure (see sketch in Fig. 1a). These time delays and frequency shifts are the origins of the loss of purity. Understanding the relationship between the loss of purity and the excitation of optical resonances of a nanostructure can be crucial for manipulating quantum information at the nanoscale.

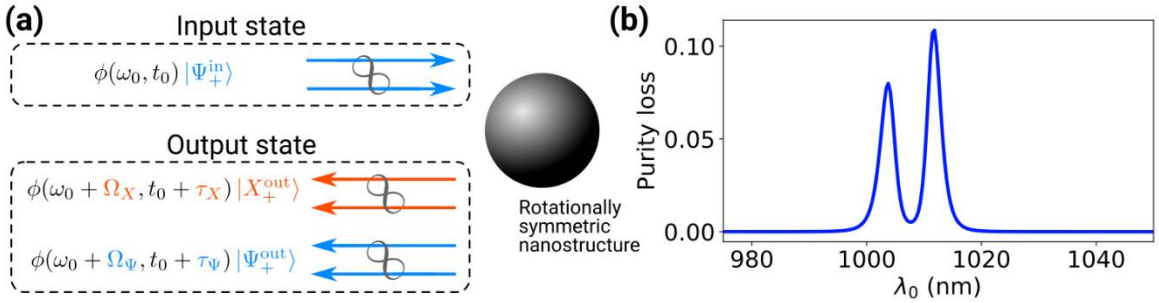

Fig. 1 Loss of purity of a two-photon state interacting with a nanostructure. (a) Sketch of the interaction. A rotationally symmetric nanostructure is illuminated by an input two-photon state $|\Psi_+^{in}\rangle$ with a Gaussian pulse envelope ϕ. The output state is given as a superposition of two states (blue and red arrows) that are frequency-shifted and time-delayed. (b) Loss of purity as a function of the central wavelength of the input $|\Psi_+^{in}\rangle$ pulse. The loss of purity is obtained considering a spherical silicon nanoparticle of radius $r = 250$ nm.

References

[1] Zambrana-Puyalto, X., and Molina-Terriza, G. 2013, J. Quant. Spectrsc. Radiat. Transf., 126, 50
[2] Molina-Terriza, G., 2008 Phys. Rev. A., 78, 053819
[3] Barnett, S.M. *et al.* 1998, Phys. Rev. A, 57, 2134
[4] Büse,A. *et. al.*, 2018, Phys. Rev. Lett., 121, 173901